ROYAL SOCIETY OF CHEMISTRY

REVIEW

Check for updates

Progress in porous metal chalcogenides for electrocatalytic water splitting

Pradnya M. Bodhankar, [a] Pradip B. Sarawade, [c] Abdulkarem I. Amhamed, [e] Tareq Al-Ansari, [de] Nawshad Haque [b] and Dattatray S. Dhawale [*b]

Industry and everyday existence are undergoing an energy structure revolution, and hydrogen is a crucial clean alternative energy source. Both academics and businesses envision water electrolysis as a key procedure for green hydrogen generation in the future. In recent years, porous metal chalcogenides (PMChs), including metal sulfides, metal selenides, and metal tellurides, have gained significant interest as electrocatalysts for electrochemical water splitting due to their distinctive structure, characteristics, and potential applications. The PMChs exhibit extensive surface areas, varied compositions, and improved electronic conductivity, rendering them exceptionally suitable for electrochemical energy conversion devices with outstanding performance. This review showcases the production of diverse PMChs by several typical methods such as hydrothermal, spray pyrolysis, electrodeposition, liquid-phase deposition, template-based, and template-free synthesis. The article also comprehensively analyzes the most recent developments in the sulfides, selenides, and tellurides for electrocatalytic water splitting (EWS). The innovative design, production, and electrochemical performance of the porous sulfide, selenide, and telluride-based metal chalcogenides are demonstrated and evaluated. Finally, the existing challenges and potential opportunities of PMChs in EWS applications are presented. We anticipate that this timely assessment will encourage more comprehensive research and generate more significant interest, thereby enhancing the advancement of potential PMChs.

1. Introduction

In the past century, global energy consumption has consistently and significantly risen due to worldwide progress and the growth of the global population. It is estimated that energy demand will increase from 16 terawatts (TW) in 2010 to 23 TW in 2030, and it may even reach 30 TW by 2050.[1] Coal, oil, and natural gas are examples of nonrenewable fossil fuels that account for more than 80% of the world's total energy consumption.[2] The quick combustion of conventional fuels dramatically contributes to the generation of CO_2, climate change, and environmental damage. Activistically implementing clean and renewable energy systems is imperative to achieve sustainable economic growth and maintain environmental equilibrium.[3] Thus, expediting the development of renewable and environmentally friendly alternatives that may effectively

address the existing issues and ensure sustainable long-term progress is essential. Given that water is the only by-product of combustion, molecular hydrogen gas (H_2) is a fuel that is very desirable since it possesses an extraordinary energy density and does not contribute to pollution. This makes it an ideal energy transporter and a promising contender for future low-carbon energy systems.[4] Electrochemical water splitting (EWS) is a promising technology for producing green hydrogen gas as an energy source, although there are already instances of sustainable energy sources being utilized.[5] The electrocatalytic half-reactions, including the oxygen evolution reaction (OER) and hydrogen evolution reaction (HER), are crucial processes in electrochemical water splitting and have been extensively researched in recent decades. The most advanced electrocatalysts for these electrochemical processes consist of noble metal and transition metal-based compounds such as Pt, IrO_2, RuO_2, and so on.[6–11] Nevertheless, the overpriced expense of the valuable electrocatalysts significantly limits their practical use. Hence, the quest for cost-effective, enduring, and affordable electrocatalysts continues to be a significant hurdle.[12,13]

Over the last several decades, there has been a growing interest in exploring transition metal chalcogenides (TMChs), more notably sulfides and selenides, as possible electrode materials for energy storage and conversion applications.[14] This is because they can have stoichiometric compositions that can

[a] *Vishwaniketan's Institute of Management Entrepreneurship and Engineering Technology, Kumbhivali, Khalapur-410203, India*

[b] *CSIRO Energy, Private Bag 10, Clayton South 3169, Victoria, Australia. E-mail: dattatray.dhawale@csiro.au*

[c] *Department of Physics, University of Mumbai, Kalina, Mumbai – 400098, India*

[d] *Division of Sustainable Development, College of Science and Engineering, Hamad Bin Khalifa University, Qatar Foundation, Doha, Qatar*

[e] *Qatar Environment and Energy Research Institute (QEERI), Hamad Bin Khalifa University, Doha 34110, Qatar*

This journal is © The Royal Society of Chemistry 2025

J. Mater. Chem. A, 2025, **13**, 22271–22294 | 22271

be adjusted, unique crystal structures, a large number of redox sites, and a comparatively better electrical conductivity compared to other catalysts and transition metal oxides.[15–17] Also, metal chalcogenides have more electrochemical reversibility than metal oxides because they have faster charge transfer kinetics. Moreover, certain metal chalcogenides such as MoS_2, CoS_2, $CoSe_2$, $FeSe_2$, *etc.*, have shown potential as electrocatalysts for HER and OER as they exhibit low overpotentials and small Tafel slopes.[18–20] Recently, porous metal chalcogenides (PMChs) have demonstrated effective electrocatalysis for both HER and OER, exhibiting enhanced activity due to their substantial internal reactive surface areas and efficient mass and electron transport through extensive pathways.[21–23]

PMChs are inorganic compounds that resemble oxide-based porous materials. The chalcogen elements—sulfur (S), selenium (Se), and tellurium (Te)—are categorized in group 16 of the periodic table, alongside oxygen (O). By altering the composition, pore dimensions, and morphology, one may proficiently adjust the properties of PMChs, encompassing conductivity and selectivity.[24] Various synthetic methodologies, such as template-assisted synthesis, self-assembly, and hydrothermal reactions, have been utilized to generate a unique porous architecture with a substantial surface area within the metal chalcogenide framework.[25,26] Furthermore, porous metal chalcogenides possess a wide range of optoelectronic properties, which vary from being insulators to genuine metals.[27,28] These properties include adjustable and significant bandgaps,

high electron mobility, and a highly polarizable surface that exhibits Lewis's basicity.[28,29] It is important to note that these qualities distinguish them from their metal-oxide counterparts. Furthermore, thorough examinations of the composition, structure, morphology, and dimensionality of porous metal chalcogenides have revealed their inherent and versatile high chemical reactivity, rendering them highly appealing for various applications, including adsorption, electrocatalysis, energy storage, and solar-to-chemical energy conversion.[30–33]

This review provides progress on porous metal chalcogenides ($MS_x/MSe_y/MTe_z$, where M represents Fe, Co, Ni, Sn, Mo, W, Sb, Mn, Zn, Cu, Ti, Ta, V, Bi, Nb, or their combinations) that are actively being explored for electrochemical water splitting reactions, namely for the HER and the OER. We begin by describing the importance of porosity and focusing on the electrocatalyst fabrication techniques and reaction mechanisms of the HER and the OER. The synthetic methods of PMChs are summarized, and their electrochemical performances are highlighted. In conclusion, the difficulties and perspectives that have been encountered in the development of PMChs for EWS are brought to light.

2. Importance of porosity

Porous materials are an essential group of substances with empty spaces, known as pores, inside their structure. The pores exhibit a diverse variety of sizes, including micropores (<2 nm), mesopores (2–50 nm), and macropores (>50 nm).[34]

Pradnya M. Bodhankar

Dr Pradnya M. Bodhankar is an Assistant Professor at the Vishwaniketan's Institute of Management Entrepreneurship and Engineering Technology, India. Dr Bodhankar obtained her PhD from the University of Mumbai, India. The primary emphasis of her ongoing research is the development of metal/metal oxide-based electrocatalysts with precise control over their shape and size for electrochemical water-splitting and advanced energy storage battery materials. In addition, Dr Bodhankar has held the position of Women Scientist (WOS-A) at the Department of Physics at the University of Mumbai, funded by a grant from the Department of Science and Technology (DST) in India. Dr Bodhankar has authored over 10 peer-reviewed journal articles, including highly cited and most downloaded review articles, which have accumulated over 500 citations in a short period.

Pradip B. Sarawade

Dr Pradip B. Sarawade has been an Assistant Professor at the Dept. of Physics, University of Mumbai, since September 2014. Before moving to Mumbai University, he served at KAUST, a catalysis center in Saudi Arabia, from 2011 to 2014. Before joining the KAUST catalysis center, he worked as a Postdoctoral Research Fellow at the Department of Chemical Engineering, Hanyang University, South Korea, from 2010–2011 and as a research scientist at E&B Nanotech Co. Ltd South Korea from 2006–2010. He obtained his PhD in Materials Science from Hanyang University, South Korea, in 2009. His research interest encompasses the development of nanomaterials like silica aerogel with enhancing specific surface area, porosity, and mechanical strength for thermal protection applications. He has co-authored more than 105 peer-reviewed publications in high-quality journals with citations of more than 3500 with an h-index of 32 and 5 patents in nanomaterials, including a book on Silica Aerogels. He is a recognized teacher at the University of Mumbai, and he guides students seeking an MSc (by research) and PhD Degrees in Physics, Chemistry, Nanosciences, and Nanotechnology.

22272 | *J. Mater. Chem. A*, 2025, **13**, 22271–22294

This journal is © The Royal Society of Chemistry 2025

Nanoporous materials refer to materials that have pore widths less than 100 nm.[35] Nanoporous metals have numerous unique characteristics that render them highly desirable as electrocatalysts.[36] The metallic structure is interconnected, forming an intensely conductive network that enables the efficient movement of electrons. Furthermore, the intricate internal curvature of the structure might expose a multitude of distinct crystal facets on the surfaces of the ligaments. This can result in advantageous reaction sites influenced by the particular reaction conditions and surface composition.[37] Moreover, the manufacturing approach can be applied to monometallic and bimetallic catalysts featuring highly porous structures and large surface areas.[36,38,39] This allows for versatility in creating and manipulating specific catalytic sites.[36] Additionally, manifolds and limited spaces inside the nanoporous structure provide a compelling approach to regulating the movement of reactants and/or products. This results in an increased preference for desirable products and reduced undesired ones. From a fundamental standpoint, the monolithic structure of nanoporous metals presents a distinct chance to separate support effects and investigate the genuine source of catalytic activity.[40,41]

Porous materials have garnered considerable attention in a range of chemical engineering processes because they have the potential to act as catalysts[42,43] Porous materials have also been widely used in electrocatalysis, a heterogeneous process that occurs at the interface.[44,45] This is because porous materials possess unique physical and chemical features that are distinct from those of ordinary materials.[42,46] As shown in Fig. 1, porous materials are adaptable in the field of electrocatalysis thanks to their ability to provide a high number of surface sites and facilitate mass diffusion during the process.

Porous counterparts can reduce the resistance to mass transfer and raise the specific current densities in HER and OER compared to bulk materials.[47,48] Over the past few years, researchers have made great strides in developing procedures for preparing a wide variety of porous structures.[49,50]

2.1 BET surface area analysis

The Brunauer–Emmett–Teller (BET) method, developed in 1938, measures surface areas of porous structures by analyzing gas molecule adsorption.[51,52] It's an extension of the Langmuir theory for multi-layer adsorption.[53] BET's simplicity and conclusiveness make it a standard tool for calculating surface areas of new porous materials, like metal chalcogenides. BET study involves injecting inert gas at boiling temperature onto porous solids, obtaining micropore volume and pore size distribution (PSD) using t-plot and Barrett–Joyner–Halenda (BJH) techniques.[54] Adsorption isotherms are classified into six types by IUPAC, providing insights into texture and pore structure explained in detail in Fig. 2 and 3.[34] By measuring N_2 multilayer adsorption, BET evaluates specific surface areas, making it a valuable tool for material characterization.

Abdulkarem I. Amhamed

Dr Abdulkarem Amhamed is the CO_2 Cluster Program Director, Principal Scientist, and Chartered Chemical Engineer with 25 years of experience in the oil and gas industry, including Industry 4.0 and sustainable process design. He holds a Doctorate in Chemical Engineering from Bradford University, UK, and an MSc from the University of Salford, UK. Currently, Dr Amhamed leads the CO_2 Cluster and Clean Fuel Program at Qatar Environment and Energy Research Institute, HBKU, Qatar Foundation. Under his leadership, the program secured $6.4 million in funding from the Qatar National Research Fund's National Priorities Research Program Cluster Track (NPRP-C) for five years. Dr Amhamed has held several senior research and management positions in both academia and industry, including serving as the Strategic Research Project Lead for a $15 million collaboration between Qatar Energy and UOP Honeywell, USA, and as the General Managing Director of ESSO Company, Libya. Dr Amahmed has authored over 70 peer-reviewed journal articles, accumulating over 1300 citations and achieving an h-index of 18 within a short period since joining the R&D division at HBKU. He also holds more than 19 patents as an inventor or co-inventor.

Nawshad Haque

Dr Nawshad Haque is a Principal Research Scientist in the Energy Business Unit at the Commonwealth Scientific and Industrial Research Organization (CSIRO) Australia and leads the Technoeconomics for Decarbonisation Team. Dr Haque also leads the India-Australia Minerals Scholar Network on Critical Minerals and Green Steel research to develop talents, which was announced as part of the joint Prime Minister's statements for both nations. Dr Haque is currently an elected Fellow of the Australian Institute of Energy, Australasian Institute of Mining and Metallurgy, and a member of TMS. Dr Haque has co-supervised over 20 CSIRO sponsored 20 PhD students and over 60 vacation scholarship projects to completion, many on technoeconomic and life cycle assessment. Dr Haque has published over 130 peer-reviewed journal articles, attracting more than 7500 citations with an h-index of 42 and an i10-index of 97, technical reports, and several book chapters. In addition, he mentors postdoctoral fellows and supervises PhD students through university and industry collaborations. Dr Haque has over 23 years of R&D experience since having a PhD in Chemical Engineering from the University of Sydney, Australia.

This journal is © The Royal Society of Chemistry 2025

J. Mater. Chem. A, 2025, **13**, 22271–22294 | **22273**

2.2 Mesoporous materials as electrocatalysts

Mesoporous materials are identified by pore diameters ranging from 2 to 50 nm.[55] Mesoporous materials possess extensive accessible surface areas and adjustable pore diameters, significantly enhancing mass transport and the dispersion of electrons and reactants. Consequently, mesoporous materials exhibit exceptional promise in electrocatalysis, photocatalysis, and energy storage and conversion.[56] The International Union of IUPAC defines a mesoporous material as having either an ordered or disordered mesostructure. In crystalline inorganic materials, the structure of mesoporous substances considerably restricts the number of lattice units, hence drastically altering the solid-state chemistry. The battery performance of mesoporous electroactive materials markedly differs from that of their bulk counterparts.[57]

Adsorption-based techniques, particularly the BET method, are employed to determine porosity and surface area because of their capacity to quantify porosity within the range of 0.4–50 nm and their measuring simplicity and cost-effectiveness. The type of isotherm (Fig. 3) can also reveal the sort, scale, and form of the pores in the material.[58]

Several porous catalysts play significant roles in the process of water splitting.[59–61] Recently, metal porous chalcogenides have emerged as a viable option to replace precious metal catalysts due to their affordability, ease of production, and inherent electronic structure for the process of water splitting.[62–64] The notable features of metal chalcogenides, derived from their diverse composition and electronic structure, include customizable active sites, rendering them excellent candidates for the development of exceptionally effective electrocatalysts.[65,66] Various metal chalcogenides materials have been shown to create functional hybrid nano-architectures using different optimization strategies, including controlling the morphology (1D, 2D, 3D, and other forms), regulating the structure (porous structure, phase regulation, amorphous structure), optimizing the electronic structure (defects, vacancies, nanointerfaces, stress regulation), and forming heterostructures with other nanomaterials (oxides, hydroxides, carbon materials, noble metals), among others.[67–69] For instance, 3D materials with mesoporous and hollow structures enhance the expression of active sites, facilitate adsorption for intermediates, and enable the release and storage of gases, rendering them promising materials across numerous fields.[70,71] The application of 3D nanostructures in electrocatalysis significantly enhances reaction efficiency due to higher contact surface area, diminished electron transfer resistance, augmented active sites, and improved connectivity between the electrolyte and catalysts. Simultaneously, the mesoporous and hollow architectures can facilitate the release of evolved gases and enhance catalytic efficacy.[17,21,72]

Tareq Al-Ansari

Dr Tareq Al-Ansari is an Associate Professor at the College of Science and Engineering, head of the sustainable development division, and acting executive director of the Qatar Environment and Energy Research Institute. He acquired a BEng. in Mechanical Engineering from the University College London and an MPhil in Engineering for Sustainable Development from the University of Cambridge. He completed his PhD in Sustainable Development and Environmental Engineering at Imperial College London. Dr Tareq Al-Ansari has authored over 150 peer-reviewed journal articles, garnering more than 12 000 citations, with an h-index of 57. His contributions also include technical reports, book chapters, and active involvement in sustainability-focused research initiatives. Dr Al-Ansari supervises PhD students through collaborative academic and industry programs and is committed to nurturing the next generation of researchers.

Dattatray S. Dhawale

Dr Dattatray S. Dhawale is a Senior Research Scientist in the Energy Business Unit at the Commonwealth Scientific and Industrial Research Organization (CSIRO), Australia's leading science agency. Dr Dhawale is a prolific, well-cited, and multiple-fellowship-winning scientist. Dr Dhawale's achievements have been honored by several prestigious fellowships, such as Brain Korea-21 (Hanyang University, South Korea), MANA NIMS Japan, Lindau Nobel Laureate Meeting, Germany, etc. Dr Dhawale led several multidisciplinary projects from idea conception to delivery. His research focuses on developing nanomaterials for next-generation electrochemical technologies for producing and utilizing clean and green fuels like hydrogen, ammonia, and CO_2 reforming to decarbonize the various energy sectors. Dr Dhawale has published over 80 peer-reviewed journal articles, attracting more than 6600 citations with an h-index of 45 and an i10-index of 67, four patents, technical reports, and several book chapters. Dr Dhawale supervises PhD students through the CSIRO Industry PhD scholarship (iPhD) program and brings together an industry partner and a university for impact-driven research. In addition, he mentors postdoctoral fellows and CSIRO-sponsored vacation students.
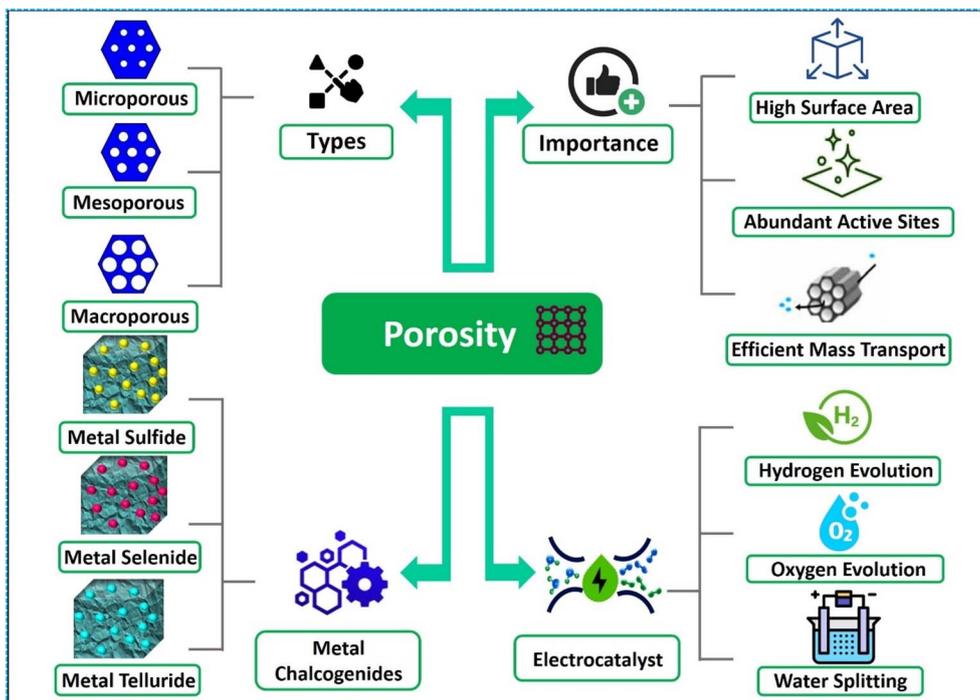
22274 | *J. Mater. Chem. A*, 2025, **13**, 22271–22294

This journal is © The Royal Society of Chemistry 2025

Fig. 1 Concept map of importance of porosity in electrochemical water splitting reactions.
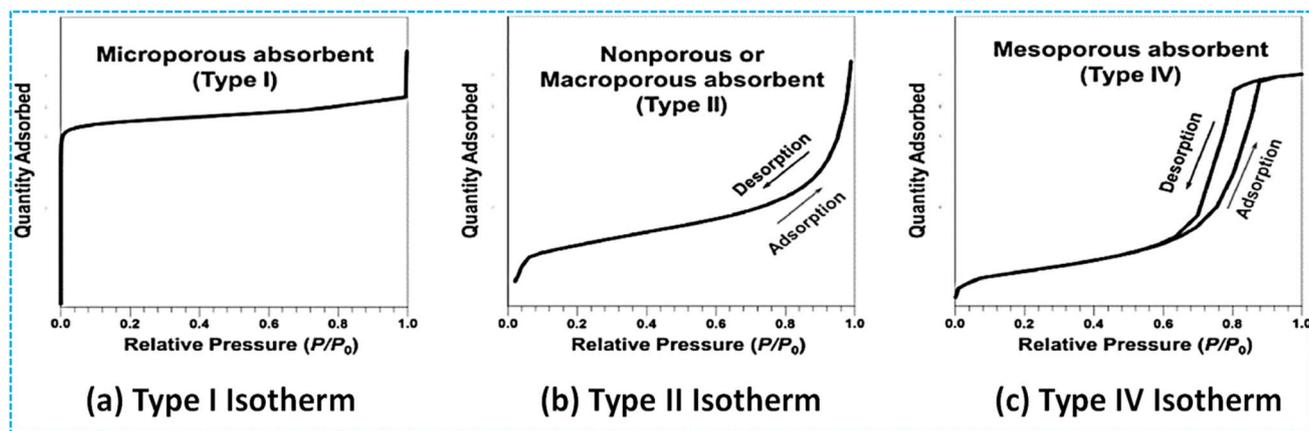

Fig. 2 The typical isotherm shapes include (a) microporous, characterized by a type I isotherm profile, (b) non-porous and macroporous, represented by a type II isotherm profile, and (c) mesoporous, which follows a type IV isotherm profile. Reproduced from ref. 34 with permission from IUPAC, copyright 1985.

It is important to note that even though metal chalcogenides have an excellent electrocatalytic performance for water splitting, it is essential to meticulously examine the alterations in morphology, structure, valence state, elemental composition, and electronic characteristics such as conductivity, bandgap, and density of states following the electrocatalytic reaction. This is because the surface of the electrocatalysts will inevitably undergo oxidation during the OER, and reduction reactions will also occur under the conditions of the HER. Hence, it is imperative to conduct a comprehensive investigation in order to verify the alterations in the electrocatalytic performance of porous metal chalcogenides that have undergone surface modification.

3. Fundamentals of electrocatalytic water splitting

Electrolysis of water uses electrical energy to separate water molecules into hydrogen and oxygen. Electrolytic water is composed of the HER and the OER. Depending on the electrolyte that is utilized, the reaction mechanism of the HER and OER can be slightly different.

3.1 Hydrogen evolution reaction (HER)

The electrochemical HER is a cathodic half-reaction that can occur through either the Volmer–Heyrovsky pathway or the
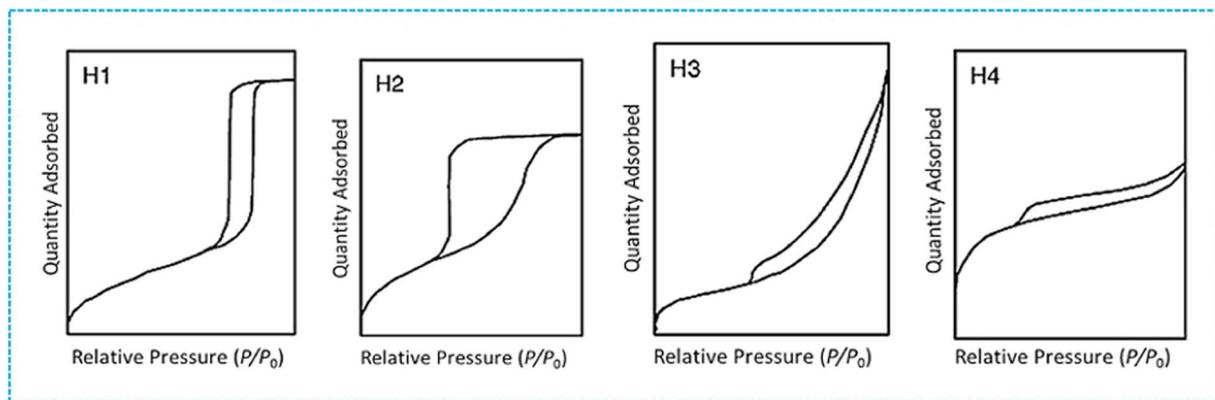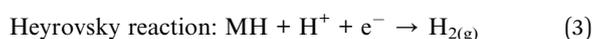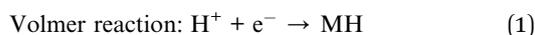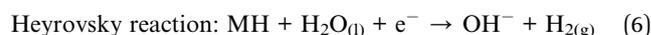
This journal is © The Royal Society of Chemistry 2025

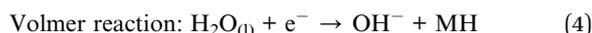J. Mater. Chem. A, 2025, **13**, 22271–22294 | **22275**

Fig. 3 The four distinct hysteresis shapes of adsorption isotherm are typically observed in subcritical N_2 adsorption studies. Reproduced from ref. 34 with permission from IUPAC, copyright 1985.

Volmer–Tafel pathway in both acidic and alkaline conditions, as seen in Fig. 4.[73] The Volmer reaction is the initial and often occurring phase, in which an electron combines with a proton that has gathered on the catalyst's surface, resulting in the formation of an adsorbed hydrogen (MH) atom intermediate. In addition, the Volmer reaction is accompanied by either the amalgamation of an adsorbed MH atom with an electron and a proton (known as the Volmer–Heyrovsky pathway) or combining two MH atoms (known as the Volmer–Tafel pathway). M represents the active sites of the catalyst. The production of the MH intermediate is implicated in both the Volmer–Heyrovsky and Volmer–Tafel pathways. The hydrogen adsorption capacity is the primary aspect considered while constructing electrocatalysts.

Acidic conditions:

$$\text{Volmer reaction: } H^+ + e^- \rightarrow MH \tag{1}$$

$$\text{Tafel reaction: } MH + MH \rightarrow H_{2(g)} \tag{2}$$

$$\text{Heyrovsky reaction: } MH + H^+ + e^- \rightarrow H_{2(g)} \tag{3}$$

Alkaline conditions:

$$\text{Volmer reaction: } H_2O_{(l)} + e^- \rightarrow OH^- + MH \tag{4}$$

$$\text{Tafel reaction: } MH + MH \rightarrow H_{2(g)} \tag{5}$$

$$\text{Heyrovsky reaction: } MH + H_2O_{(l)} + e^- \rightarrow OH^- + H_{2(g)} \tag{6}$$

Individual steps can serve as rate-determining reactions that dictate the HER rate within various reaction processes. Enhancing the speed of these reactions is crucial for optimizing the overall water-splitting.

3.2 Oxygen evolution reaction (OER)

OER, is a chemical process that involves the transfer of four electrons. The standard potential of OER is 1.23 V *vs.* RHE. Kinetically, the simultaneous transmission of several electrons is not beneficial.
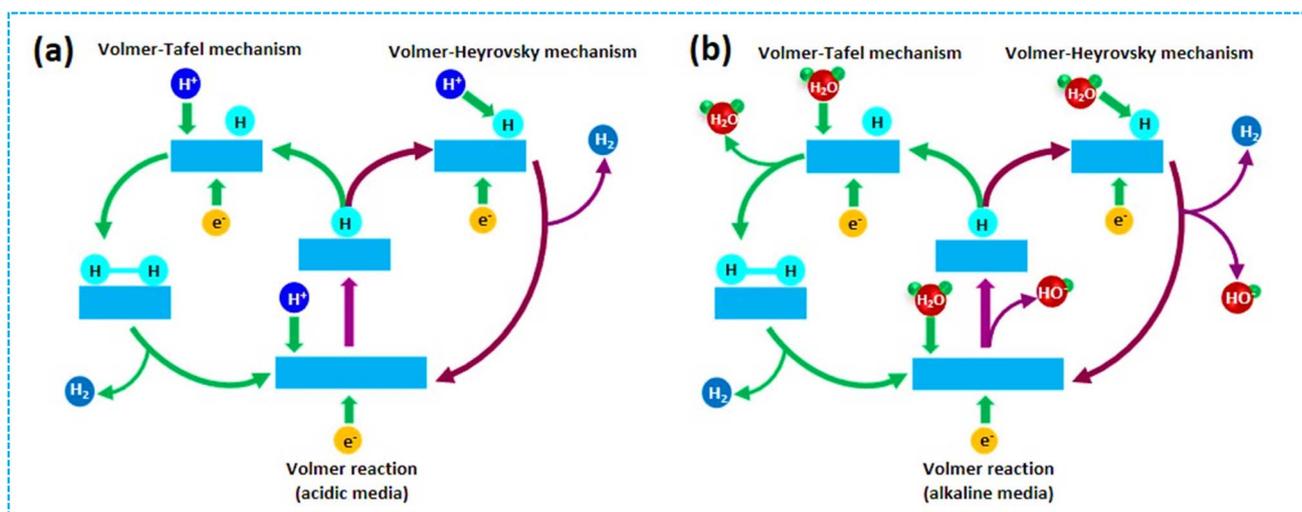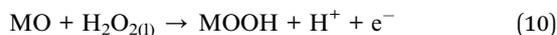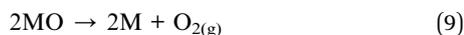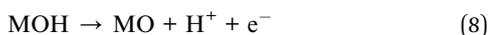

Fig. 4 Schematic representation of HER mechanism in (a) acidic and (b) alkaline media.

Acidic conditions:

$$M + H_2O_{(l)} \rightarrow MOH + H^+ + e^- \tag{7}$$

$$MOH \rightarrow MO + H^+ + e^- \tag{8}$$

$$2MO \rightarrow 2M + O_{2(g)} \tag{9}$$

$$MO + H_2O_{2(l)} \rightarrow MOOH + H^+ + e^- \tag{10}$$

$$MOOH \rightarrow M + O_{2(g)} + H^+ + e^- \tag{11}$$

Alkaline conditions:

$$M + O^- \rightarrow MOH + e^- \tag{12}$$

$$MOH + OH^- \rightarrow MO + H_2O_{(l)} + e^- \tag{13}$$

$$2MO \rightarrow 2M + O_{2(g)} \tag{14}$$

$$MO + OH^- \rightarrow MOOH + e^- \tag{15}$$

$$MOOH + OH^- \rightarrow M + O_{2(g)} + H_2O_{(l)} + e^- \tag{16}$$
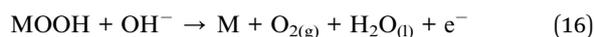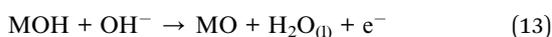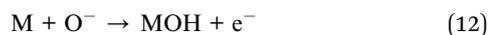
Within the OER process, every individual step must surpass a substantial variation in potential, leading to the slow kinetics of OER. The reaction mechanism is illustrated in Fig. 5. To achieve efficient water electrolysis, it is imperative to tune the anode catalyst and minimize the overpotential of the OER.

The OER refers to the half-reaction involved in the process of water splitting. The processes occurring at the cathode and anode during the water-splitting reaction exhibit distinct characteristics in both acidic and alkaline environments. Several research groups have suggested various processes for the OER at the anode electrode, either in acidic conditions (eqn (7)–(11)) or alkaline settings (eqn (12)–(16)). There are both differences and commonalities among these proposed mechanisms. The majority of the hypothesized pathways share common intermediates, such as MOH and MO. However, the main distinction is in the reaction that produces oxygen. There are two distinct methods for producing oxygen from a MO intermediate, as shown in Fig. 5. The initial pathway necessitates the direct amalgamation of 2MO to yield $O_{2(g)}$. The alternative path entails

the synthesis of the MOOH intermediate, which subsequently undergoes decomposition to produce $O_2(g)$. This second route is represented by the black line in Fig. 5. While distinctions exist, there is widespread agreement that the electrocatalysis of OER constitutes a heterogeneous process, wherein the bonding interactions (M–O) among the intermediates (MOH, MO, and MOOH) are crucial to the overall electrocatalytic efficacy. An electrocatalyst is a catalyst that aids in electrochemical reactions. The material may be modified either at the electrode's surface or function as the electrode itself. In general, the primary role of the electrocatalyst is to attract the reactant onto its surface, resulting in the formation of an adsorbed intermediate. This process aids in transferring charge between the electrode and the reactant.

3.3 Criteria for electrochemical water splitting performance evaluation

Electrocatalytic activity can be assessed using several fundamental characteristics, including overpotential (η), Tafel slope, exchange current density, electrochemical impedance spectroscopy, electroactive surface area, turnover frequency (TOF), and stability. The catalyst was evaluated using linear scan voltammetry (LSV). Typically, the overpotential value at 10 mA cm^{-2} is lower, indicating a lower voltage for hydrogen production by water decomposition.

3.3.1 Overpotential (η). Overpotential (η) is a crucial factor for assessing the performance of electrocatalysts in water splitting. It is among the most significant criteria to consider in evaluating their performance. Overpotential, in theory, is the discrepancy between the real potential and the thermodynamic value at a certain current density (eqn (17)).[74] The theoretical potentials for HER and OER are 0 volts and 1.23 volts, respectively, as stated previously. However, in practice, the slow reaction rates of the HER and OER necessitate the use of a larger applied potential to overcome the inherent energy barrier throughout the catalytic process.

$$\eta = E_{applied} - E_0 - iR \tag{17}$$

where, $E_{applied}$ represents the actual applied potential, E_0 is the theoretical equilibrium value, and iR denotes the ohmic correction under similar conditions.
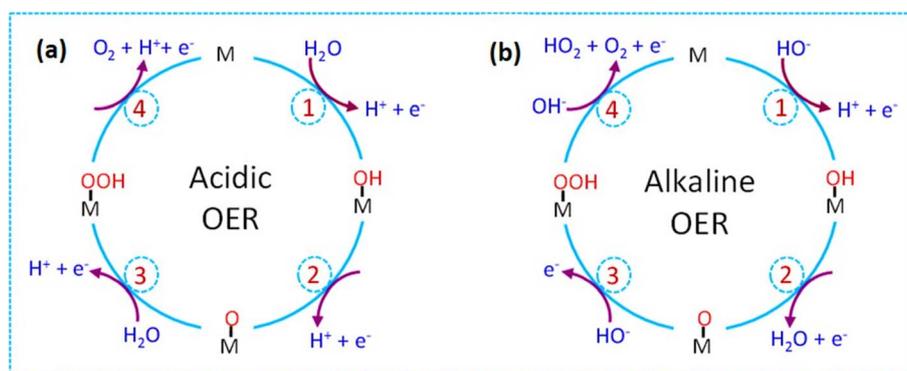

Fig. 5 Schematic representation of OER mechanism in (a) acidic and (b) alkaline media.

The electrocatalytic activity of a catalyst is typically evaluated using three overpotential values obtained from the polarisation curve at current densities of 1 mA cm^{-2} (η_1), 10 mA cm^{-2} (η_{10}), and 100 mA cm^{-2} (η_{100}). The initiation of the reaction is often indicated as η_1. The standard for comparing the performance of electrocatalysts is always represented by the value of η_{10}. This is to get a photoelectrochemical water splitting efficiency of 12.3%.[75] However, it is important to mention that the overpotential is highly influenced by the amount of active material loaded on the electrode. Therefore, to make a fair comparison of the activity of different electrocatalysts, it is advised that the amount of loading mass be normalized based on the surface area of the electrode.[76] In addition, a value of 100 for η is a crucial factor to consider when evaluating practical applications.

3.3.2 Tafel slope (b). The Tafel slope (b) is a crucial metric indicating the water-splitting activity level. The Tafel slope measures the rate at which the current density increases as the overpotential increases. It is used to analyze the kinetics of an electrocatalyst. In general, there is a logarithmic relationship between overpotential and current density. According to the Tafel equation (eqn (18)), the Tafel slope can be linearly fitted on the Tafel plot with the expression:

$$\eta = a + b \log j \tag{18}$$

where η represents the overpotential, b represents the Tafel slope, and j represents the current density.[77] The Tafel diagram provides us with another significant quantity known as the exchange current density (j_o). When the value of η is zero, the corresponding current density (j) is referred to as the exchange current density (j_o). Generally, a high turnover frequency (j_o) and a lower Tafel slope indicate better catalytic activity.

3.3.3 Turnover frequency (TOF). The term "TOF" refers to the number of molecules that transform to produce the desired product at each active site during a specific period. It exposes the inherent activity of electrocatalysts. The TOF values can be determined using eqn (19).[78]

$$\text{TOF} = \frac{jA}{\alpha Fn} \tag{19}$$

where j represents the current density in the polarisation curve, A is the surface area of the working electrode, α is the number of electrons generated per molar of the target product in the HER or OER reaction, F is the Faraday constant, and n is the number of moles of the active materials. Calculating the TOF value accurately is particularly challenging due to the unequal catalytic activity of atoms inside a catalyst. Nevertheless, TOF remains a valuable metric for comparing similar catalysts.

3.3.4 Stability. Stability is an essential consideration in assessing the longevity of a catalyst for real-world use. Typically, two approaches are employed to determine the stability of electrocatalysts.[79] Firstly, a cyclic voltammetry measurement is conducted by comparing the polarisation curve of the catalyst before and after 1000 cycles of cyclic voltammetry. In general, if the overpotential closely aligns with the initial polarisation curve, it indicates a high level of stability. Another approach

involves the utilization of chronoamperometry or chronopotentiometry for measurement purposes. The rate of change in electrical potential over a certain period can be quantified at a designated level of electric current, where a high degree of preservation indicates exceptional stability.

4. Synthesis of porous metal chalcogenides

Porous metal chalcogenides (PMChs) are a series of high-performance water-splitting catalysts that are based on earth-abundant metals.[80,81] Recently, it has been discovered that these catalysts are readily available and highly active.[14,24,82] The notable attributes of metal chalcogenides, such as their regulated shape and many active sites, contribute to their high reactivity, making them an excellent choice for constructing hybrid nanomaterials. Typically, metal chalcogenides can be synthesized *via* solid-phase chemical synthesis, wet-chemical synthesis, or a chemical vapor deposition (CVD) – based epitaxial growth technique. In developing multifunctional metal chalcogenides and hybrid nanostructures derived from these compounds, numerous strategies can be employed to modify their physical and chemical properties, providing a wide range of applications.

4.1 Porous metal sulfides

Transition metal sulfide materials are becoming increasingly popular in electrochemical energy storage and conversion due to their favorable electrical characteristics and affordable cost.[83,84] Mesoporous metal sulfides are the most intriguing of all metal sulfides. Mesoporous materials offer several benefits, including extremely high surface areas, adjustable mesopores, and large pore volumes. These characteristics enhance the active surface, facilitate the movement of guest species through the material, and alleviate structural strain caused by volume expansion resulting from redox reactions.[85] Significant actions have been undertaken to synthesize mesoporous metal sulfides.[86–89] The early efforts have been made using soft templating methods, sol–gel, and aerogel.[90–92] The most generally used method for producing well-structured mesoporous metal sulfides is nanocasting, which employs mesoporous silica as a rigid template.[88,93] Using thermally stable hard templates enables the successful production of highly crystalline mesoporous metal sulfides.

A rapid one-step flame combustion deposition approach was devised by Wang *et al.*[94] The method involved fabricating mesoporous metal sulfides directly on nickel foam without the use of a binder or template (Fig. 6a). The first-row transition metal sulfides, which include Co_9S_8, Ni_3S_4, $NiCo_2S_4$, and FeS, were successfully synthesized using a three-dimensional architecture, a large specific surface area (about 110 m^2 g^{-1}), and interconnected pore networks. This study presented a novel and scalable approach to acquire mesoporous metal sulfides that exhibit exceptional electrochemical performance.[94] The synthesis of mesoporous transition metal dichalcogenides greatly relies on this practical approach, which is of

22278 | *J. Mater. Chem. A*, 2025, **13**, 22271–22294

This journal is © The Royal Society of Chemistry 2025
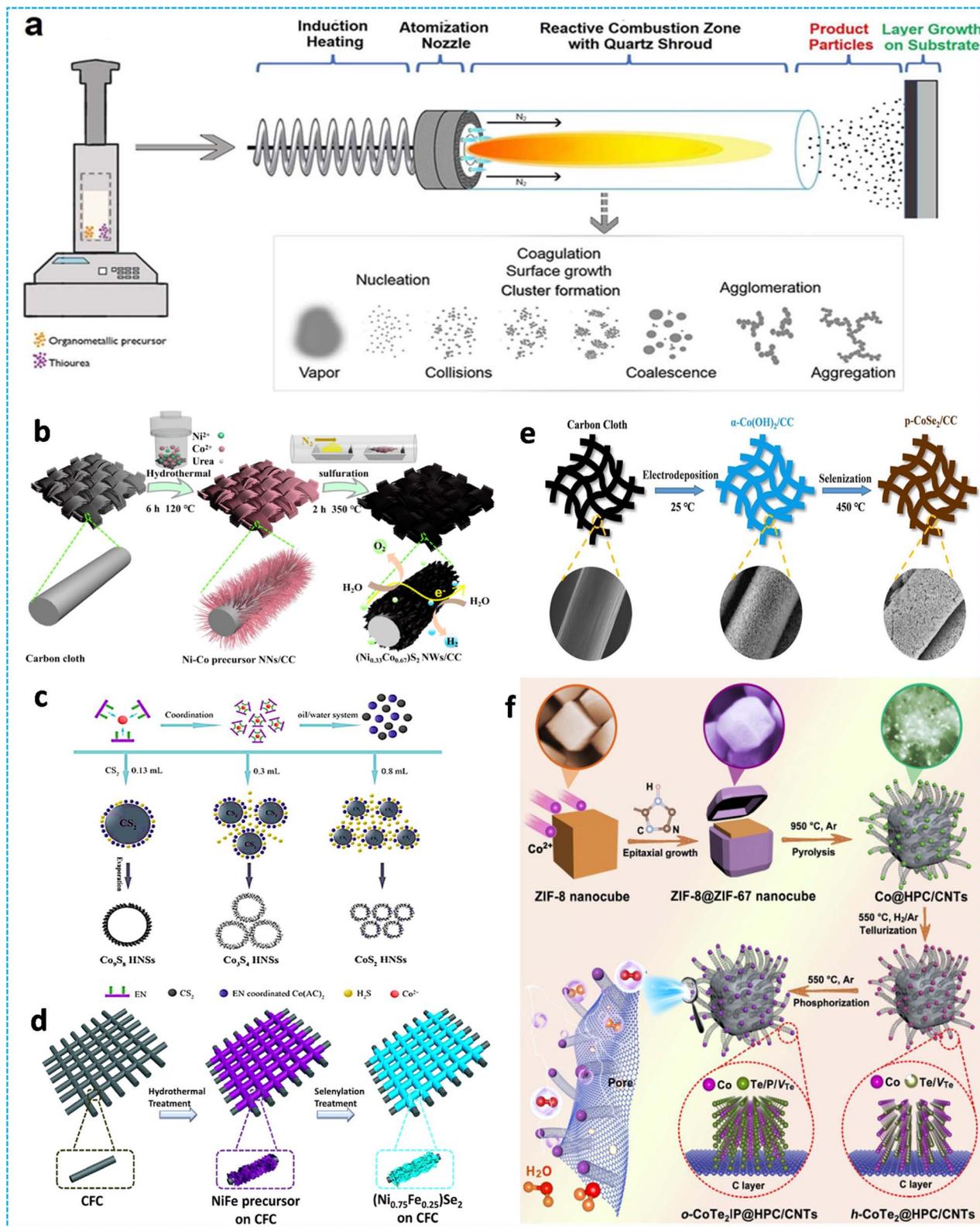
Fig. 6 (a) Schematic representation of the reactive spray deposition process for mesoporous metal sulfides. Reproduced from ref. 94 with permission from American Chemical Society, copyright 2019. (b) Schematic representation of the fabrication process for $(Ni_{0.33}Co_{0.67})S_2$ NWs/ CC. Reproduced from ref. 95 with permission from American Chemical Society, copyright 2018. (c) Schematic representation of the synthetic methodologies of Co_9S_8, Co_3S_4, and CoS_2 HNSs, respectively. Reproduced from ref. 96 with permission from Royal Society of Chemistry, copyright 2018. (d) Schematic illustration of the synthesis procedures for porous $(Ni_{0.75}Fe_{0.25})Se_2$ nanosheets on CFC. Reproduced from ref. 97 with permission from American Chemical Society, copyright 2016. (e) Schematic illustration of the synthesis of p-CoSe$_2$ on carbon cloth. Reproduced from ref. 98 with permission from American Chemical Society, copyright 2018. (f) Schematic illustration for the synthesis of o-CoTe$_2$|P@HPC/CNTs composite. Reproduced from ref. 99 with permission from American Chemical Society, copyright 2020.

fundamental significance. Zhang et al.[95] have synthesized a distinctive three-dimensional catalyst consisting of inter-connected porous networks of NiCo disulfide that were grown on carbon cloth (CC).[95] This was achieved by a simple hydro-thermal technique followed by a low-temperature sulfuration process. The process of creating a network of linked pores in $(Ni_{0.33}Co_{0.67})S_2$ nanowires (NWs) on a carbon cloth substrate is depicted in Fig. 6b. The nitrogen adsorption–desorption isotherm plot of $(Ni_{0.33}Co_{0.67})S_2$ NWs exhibits a type IV isotherm, indicative of mesopore existence. Comparing the BJH pore size distribution curves reveals that the average pore size of NiCo precursor NNs is 1.2 nm, but that of $(Ni_{0.33}Co_{0.67})S_2$ NWs is 9.1 nm, further confirming their mesoporous nature. The specific surface area of the $(Ni_{0.33}Co_{0.67})S_2$ nanowires, as measured by the BET method, was 24.61 $m^2 g^{-1}$. This value was considerably higher than the specific surface area of the NiCo precursor nanoneedles, which was 5.57 $m^2 g^{-1}$. The presence of a mesoporous structure and a larger surface area resulted in the exposure of a significant number of active sites. This leads to an increase in the contact area between the electrode and electro-lyte, hence enhancing the rate of electron diffusion.[95] Ma et al.[96] have successfully created three CoS_x compounds, specifically Co_9S_8, Co_3S_4, and CoS_2 hollow nanospheres (HNSs), by accu-rately changing the molar ratio of carbon disulfide to cobalt acetate in a facile solution-based approach.[96] Fig. 6c displayed a schematic representation of the preparation process. The Co_9S_8, Co_3S_4, and CoS_2 hollow nanospheres were synthesized using a simple wet-chemical process. The CS_2 served as both a sulfur supply and an oil-droplet template in the reaction. Usually, three ethylenediamine (EN) molecules react with

a cobalt ion (Co^{2+}) to produce a complex solution called $[Co(EN)_3]^{2+}$. Subsequently, when this solution is mixed with an aqueous solution and carbon disulfide (CS_2), it forms an oil/water system. Subsequently, EN interacts with the CS_2 oil phase, resulting in the liberation of H_2S at the interface between oil and water. Subsequently, hydrogen sulfide (H_2S) can undergo a reaction with $[Co(EN)_3]^{2+}$ to generate nuclei of cobalt sulfide. The excess CS_2 evaporated, and the hollow nano-spheres, constructed from nanosheets, were ultimately ob-tained. The CoS_2 HNSs exhibit a markedly greater BET surface area (71.2 $m^2 g^{-1}$) compared to the other two comparatives, hence offering an increased number of electroactive sites and enhancing electrolyte penetration in the catalytic process.[96]

4.2 Porous metal selenides

Among the group of transition metal chalcogenides, metal selenides (Se) have recently been identified as a distinct family of compounds for water electrolysis. They possess particular characteristics that set them apart from their sulfide counter-parts, commonly called "star chalcogenides". The 3d orbital of Se can bond with metal atoms since its energy level is close to the 3s and 3p orbitals. The electron structure of transition metal selenides promotes increased metallicity, which enhances electron transport and facilitates chemical reactions. In addi-tion, porous metal selenides provide several benefits, including easy preparation, exceptional catalytic activity, and outstanding stability. These qualities make them very suitable for the elec-trochemical breakdown of water, making them perfect candi-dates for this process. Wang et al.[97] presented a study where they described a simple technique for creating porous

Table 1 Synthesis methods, porosity, BET surface area and pore size of porous metal chalcogenides

Porous metal chalcogenides	Synthesis method	Morphology	Porosity	BET surface area ($m^2 g^{-1}$)	Pore size (nm)	Ref.
NiS/Ni/NC	Ball-milling	Sponge-like	Meso-	921.2	4	100
CoS_x	Anodization	Wrinkled-like	Meso-	35.6	5	101
$MoS_2/CoMo_2S_4$	Soft template	Spherical	Meso-	53	7	102
FeS_2	Sol–gel	Spherical	Meso-	128	3.8	21
Co_9S_8	Reactive spray deposition	Coral-reef-like	Meso-	120	4.8	94
Ni_3S_4				118	5.3	
$NiCo_2S_4$				113	5.6	
FeS				101	6.3	
$Ni_{0.76}Fe_{0.24}Se$	Hydrothermal	3D-rose-like	Meso-	14.3	5.2	22
$Cu_{0.4}Ni_{0.3}Co_{0.3}Se_2$@N-C n-box	Template-assisted refluxing method	Hollow nanobox	Meso-	72.1	2.5	103
$Ni_{0.5}Mo_{0.5}OSe$	Hydrothermal	Nanosheets	Nano-	286	2.36	104
Co/Fe/Se-400	Solvothermal	2D lamellar structure	Micro-	178.72	2.40	105
CoZn–Se	Liquid-phase deposition	Nanoflakes	Porous	20.4	7.9	106
$O-Co_{0.5}Mo_{0.5}Se_2$	Hydrothermal	Nanoflakes	Nano-	302	3.59	107
Ni-MOF-Fe-Se-400	Solvothermal	Nanosheet and mesoporous tubes	Meso-	86.86	3	108
$CoTe_2$@CdTe	Hydrothermal	Nanowire array	Meso-	18.28	31.1	109
CoTe	Hydrothermal	Nanoflakes	Porous	53.4	—	110
$NiNCs-1T-Mn-VTe_2$	Hydrothermal	Nanosheet	Meso-	92	24.3	111
$CoTe_2/MnTe_2$	Hydrothermal	Nanorods	Porous	134.9	6.8	112
$V-CoTe_2/MoTe_2$@CC	Hydrothermal	Nanodendrites	Meso-	279.5	5.5	113
NdTe-HS/NF	Hydrothermal	Hollow shell	Meso-	43	—	114

22280 | J. Mater. Chem. A, 2025, **13**, 22271–22294

This journal is © The Royal Society of Chemistry 2025

$(Ni_{0.75}Fe_{0.25})Se_2$ nanosheets on flexible and conductive CFC support material (Fig. 6d).[97] Initially, the ultrathin NiFe-based nanosheet precursor was created using a standard solvothermal method. Subsequently, the porous $(Ni_{0.75}Fe_{0.25})Se_2$ nanosheets with a high surface area of 60.3 m^2 g^{-1} were obtained by directly subjecting the precursor to a secondary hydrothermal procedure, including selenisation. The fabricated porous $(Ni_{0.75}Fe_{0.25})Se_2$ nanosheets showed superior electrochemical performance (overpotential of 255 mV at 35 mA cm^2 and a low Tafel slope of 47.2 mV dec^{-1}) compared to the nanosheet precursors based on Ni, NiFe, and porous $NiSe_2$. The excellent performance of the $(Ni_{0.75}Fe_{0.25})Se_2$ nanosheets can be due to their porous nanostructure, high electronic conductivity, and extensive electro-active surface area resulting from the integration of Fe and the process of selenisation.[97] Although recent improvements have been made in creating transition metal selenide nanostructures, making a porous nanosheet electrode without a binder with more active sites is still challenging. Wan et al.[98] described the vapor selenisation of a pre-synthesized α-$Co(OH)_2$ nanosheet array precursor, resulting in the self-templating production of a porous $CoSe_2$ nanosheet array on carbon cloth (p-$CoSe_2$/CC).[98] As depicted in Fig. 6e, the synthetic procedures can be separated into two distinct stages: (i) the α-$Co(OH)_2$ nanosheets are grown on CC by electrodeposition at 25 °C. (ii) The α-$Co(OH)_2$/CC is converted to p-$CoSe_2$/CC by reacting with selenium vapor at a temperature of 450 °C. The material demonstrated a significant active surface area, rapid diffusion of produced gas, and robust structural stability during electrochemical water-splitting reactions (Table 1).[98]

4.3 Porous metal tellurides

Transition metal tellurides (TMTs) have gained significant interest as emerging catalysts due to the unique properties of tellurium (Te). In comparison to other chalcogens like selenium (Se), sulfur (S), and oxygen (O), tellurium (Te) has a lower electronegativity and a more metallic nature.[115] These characteristics contribute to improved electrical conductivity and a stronger covalent bond between the metal and chalcogen atoms in TMTs. The covalent character in the system can result in a beneficial electronic band structure. This makes it easier to establish the boundaries of the valence band and the conduction band with the oxidation and reduction potentials of water that are present. In addition to this, it enhances the redox reactions that occur within the transition metal center, which ultimately results in an improvement in the electrocatalytic performance.[23,116,117] Chen et al.[99] found that vacancy occupation triggers a phase change from hexagonal to orthorhombic $CoTe_2$, significantly increasing OER catalytic activity. To create h-$CoTe_2$@HPC/CNTs, hexagonal $CoTe_2$ nanoparticles with high Te-vacancy content were pyrolyzed and then tellurized in core–shell ZnCo-zeolitic imidazolate frameworks. $CoTe_2$ underwent a polymorphic transition from hexagonal to orthorhombic structure through anion P-doping (Fig. 6f). This resulted in the creation of HPC/CNTs-confined orthorhombic P-doped $CoTe_2$ nanoparticles (o-$CoTe_2$|P@HPC/CNTs). Hierarchically porous carbon was designed to maximize surface area and prevent nanoparticle agglomeration. The BET

surface area and pore volume of o-$CoTe_2$|P@HPC/CNTs were calculated as 262 m^2 g^{-1} and 0.362 cm^3 g^{-1}, respectively. Large BET surface area and well-distributed pores can expose active areas and speed up mass diffusion during electrochemical reactions.[99] Xue et al.[118] fabricated NiTe nanoarrays arranged in a cross-columnar pattern supported on a nickel foam substrate.[118] Etching nickel foam using sodium tellurite as a source of tellurium and hydrazine hydrate as the reducing agent was the method that was utilized in the fabrication of the NiTe nanoarrays on NF. This process generated tellurium ions in a hydrothermal system at a temperature of 180 °C for a duration of 24 hours. Afterward, an ion exchange method was employed to create NiTe/NiS heterojunctions. This involved immersing the NiTe nanoarrays in a sodium sulfide solution at a temperature of 160 °C for a duration of 8 hours. Remarkably, the NiTe/NiS nanoarrays, demonstrated exceptional stability and displayed remarkable activity in the OER at extremely low overpotentials.[118] Xu et al.[119] aimed to create a new Ni_3Te_2–CoTe composite electrocatalyst in their study, considering the benefits of the hybridization approach.[119] The Ni_3Te_2–CoTe composite was synthesized on carbon fabric using a one-step hydrothermal method. Adding CoTe in Ni_3Te_2–CoTe/CC enhanced the exposure of Ni_3Te_2, contributing to a superior catalytic performance. The results indicated that Ni_3Te_2–CoTe/CC has the potential to be a suitable option for many applications requiring OER. Furthermore, the findings demonstrated that using material hybridization as a straightforward and efficient approach to improve the electrochemical performance of an electrode was a significant finding.[119]

5. Electrocatalytic water splitting performance of porous metal chalcogenides

Electrocatalysis is gaining importance in sustainable technologies as the demand for alternative energy sources, especially in green energy conversion and clean fuel production sectors, continues to rise.[120–122] Electrocatalytic water-splitting, powered by renewable energy, is highly regarded as a significant achievement in the future energy sector.[123,124] This process utilizes water, a renewable resource, to produce H_2, which has a high energy content of 143 MJ kg^{-1} and is a clean energy carrier with zero carbon emissions.[125,126] A variety of metal chalcogenides, such as CoS_2, FeS_2, NiS_2, MoS_2, CoTe, NiSe, etc., have been effectively produced as porous structures with diverse morphologies, crystal phases, and pore size distributions.[20,21,127–135] In this section, we examine the electrochemical energy uses of common porous metal chalcogenides. These materials are appealing due to their notable characteristics, such as strong mechanical properties, high stability against heat and chemicals, compatibility with the environment, versatile surface chemistry, and diverse architecture. Additionally, they possess a significant number of oxygen vacancies and defects. The article also demonstrates the appropriate configuration of micropores, mesopores, and macropores, which can serve as chemical reaction regions.

This journal is © The Royal Society of Chemistry 2025

J. Mater. Chem. A, 2025, 13, 22271–22294 | 22281

5.1 Porous metal sulfides for EWS

Until now, nickel sulfide has been well-researched and suggested to be effective in electrocatalytic water splitting in an alkaline media.[136,137] To further enhance the catalytic activity, NiS_2 has been combined with a highly efficient electrocatalyst,

such as MoS_2, resulting in increased catalytic activity.[138] Lonkar et al.[138] have suggested an eco-friendly method for synthesizing MoS_2-wrapped NiS_2 nanohybrids that were evenly distributed on conductive graphene sheets. Fig. 7a depicts the scheme for creating mesoporous MoS_2–NiS_2/G nanohybrids using solid-
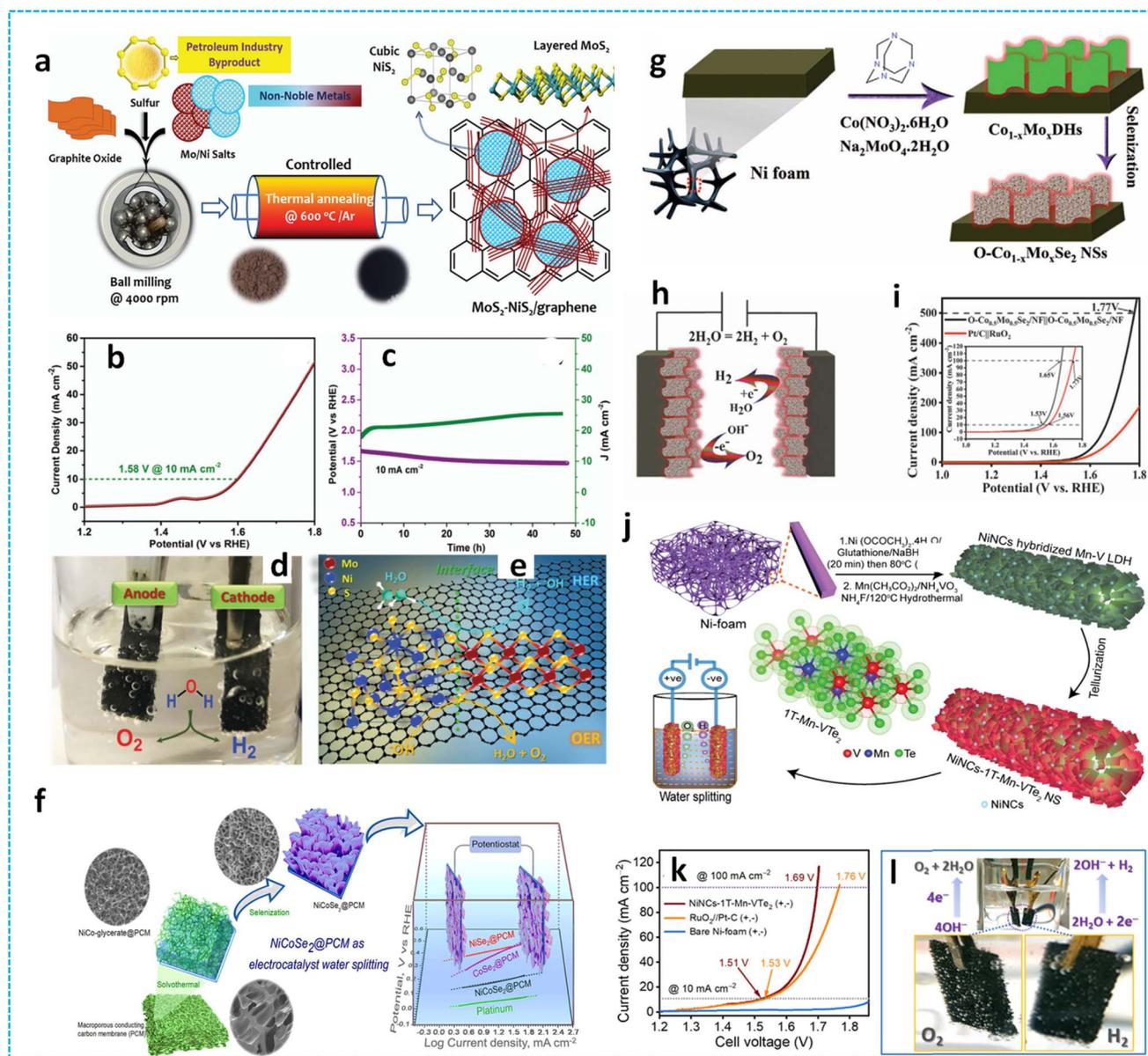

Fig. 7 (a) Schematic showing of the fabrication of the MoS_2–NiS_2/G nanohybrid, (b) the cathode and anode LSV curves of the MoS_2–NiS_2/G||MoS_2–NiS_2/G two-electrode system in 1 M KOH, (c) chronopotentiometry and chrono-amperometry curves at a constant current density of 10 mA cm^{-2} and potential for overall water splitting, (d) an optical photograph illustrating the production of hydrogen and oxygen bubbles resulting from the overall water splitting process on MoS_2–NiS_2/G, functioning as both the anode and cathode and (e) schematic illustration of the overall water splitting using MoS_2–NiS_2/G as a bifunctional electrocatalyst for simultaneous HER and OER. Reproduced from ref. 138 with permission from Royal Society of Chemistry, copyright 2020. (f) Table of contents graphic of 3D binder-free $NiCoSe_2$@PCM as a high-efficiency bifunctional electrocatalyst for overall water splitting. Reproduced from ref. 149 with permission from Elsevier, copyright 2021. (g) Schematic illustration for the design and fabrication of the O-$Co_{1-x}Mo_xSe_2$ ($0 \le x \le 1$) nanostructures, (h) schematic representation for the construction of water splitting device, (i) polarization curves of O-$Co_{0.5}Mo_{0.5}Se_2$||O-$Co_{0.5}Mo_{0.5}Se_2$ and Pt/C||RuO_2 devices at a fixed scan rate of 10 mV s^{-1}. Reproduced from ref. 107 with permission from Wiley, copyright 2020. (j) Schematic of the construction of the NiNCs-1T-Mn-VTe_2 NS and its utilization as a superior electrocatalyst for overall water splitting, (k) LSV measurements curves of NiNCs-1T-Mn-VTe_2, (l) digital NiNCs-1T-Mn-VTe_2 image of the device during the electro-catalytic water splitting showing the appearance of H_2 reaction and O_2 gas bubbles on the surface of the cathode and anode. Reproduced from ref. 111 with permission from Elsevier, copyright 2022.

22282 | J. Mater. Chem. A, 2025, 13, 22271–22294

This journal is © The Royal Society of Chemistry 2025

state synthesis. These nanohybrids were utilized as a bifunctional electrocatalyst for the process of overall water splitting (Fig. 7b). The combination of MoS_2–NiS_2/graphene has resulted in an increased surface area (105 m^2 g^{-1}), many electro-active sites, and a customized conductive network. This has led to improved efficiency in the process of water splitting. The nanohybrid demonstrated excellent catalytic efficiency for the HER with remarkably low overpotentials in both acidic (152 mV) and alkaline (141 mV) environments at a current density of 10 mA cm^{-2}. Similarly, a low OER overpotential of 320 mV was attained in an alkaline environment. The resulting nanohybrid has developed into a highly effective electrocatalyst with dual functions, allowing efficient water splitting. It achieves a final cell voltage of 1.58 V and demonstrates excellent activity and stability (Fig. 7c). As shown in Fig. 7d, hydrogen and oxygen evolved significantly at the cathode and the anode electrodes. MoS_2–NiS_2/G possesses outstanding electrocatalytic performance, which can be attributed to the presence of a heterogeneous nanostructure composed of MoS_2 and NiS_2. In addition to being supported by a conductive graphene framework, this nanostructure was loaded with defect-rich synergistic interfaces. This arrangement provides a large number of active sites and ensures high-rate and long-life stability, as shown in Fig. 7e.[138] Previous research has shown that porous cobalt sulfides, such as Co_9S_8, CoS_2, CoS, etc., exhibit superior catalytic activity for both the HER and the OER in an alkaline media.[127,139–141] Additionally, these sulfides demonstrate exceptional chemical stability and electrical conductivity. Moreover, earlier research has shown that the free energy of adsorption for hydrogen and oxygen-containing substances decreases when cobalt atoms are added to the edge sites of other transition metal chalcogenides.[142,143] Furthermore, the transfer of charge inside the electrocatalyst material through linkages, as well as between the electrocatalyst interface and species containing H and O, is enhanced synergistically, thereby showing a considerable increase in the catalyzing activity of HER and OER.[142] Further, the combination of porous cobalt and nickel sulfide shows potential for use in electrocatalytic water splitting.

Moreover, increasing the intrinsic activity towards HER and OER can be accomplished by utilizing a porous heterostructured nanoelectrocatalyst, which provides a potential technique.[144–147] For instance, Hu et al.[148] created freestanding heterogeneous CoS_2/CoS nanosheets using a one-step sintering procedure. These nanosheets were made using a unique hierarchical tremella-like metal–organic framework (MOF) and exhibited a high specific surface area of 45.35 m^2 g^{-1}. A cost-effective OER electrocatalyst has been developed, which produces satisfactory electrocatalytic efficiencies with a low overpotential of 269 mV at a current density of 10 mA cm^{-2}, a Tafel slope of 52 mV dec^{-1}, and a good stability in alkaline solution that is comparable to that of RuO_2 counterparts.[148] Ran et al.[21] described a simple synthetic procedure for creating mesoporous FeS_2 as an electrocatalyst for the HER without using a hard template. After a sulphurization process in an H_2S environment, the sol–gel method was used to successfully generate the mesoporous FeS_2 materials with a high surface area (128 m^2 g^{-1}).

An impressive HER catalytic performance was attained with a low overpotential of 96 mV at a current density of 10 mA cm^{-2} and a Tafel slope of 78 mV per decade in alkaline circumstances (pH 13). According to theoretical estimates, the exposed (210) facets are responsible for the mesoporous FeS_2's exceptional catalytic activity. The mesoporous FeS_2 material may offer a viable substitute for Pt-based electrocatalysts for water splitting.[21] Yang et al.[150] described a three-dimensional (3D) porous CoS_2/FeS-MOF with tunable Co/Fe molar ratios for HER and OER (CoS_2/FeS-MOF@NF). The built symmetric electrolyzer CoS_2/FeS-MOF@NF-1 achieves a low cell voltage of 1.5 V at 10 mA cm^{-2} and long-term stability for 24 hours.[150]

Another research proposes a design methodology for effective high-current-density OER electrocatalysts utilizing sustainable wood fiber materials.[151] The researchers enclosed Co_9S_8/CoS heterojunction nanoparticles within a sulfur and nitrogen co-doped carbon (SNC) matrix and uniformly attached them onto the S-doped carbonized wood fibers (SCWF) substrate to create microleaf arrays. The heterojunction interface effect in (Co_9S_8/CoS)@SNC can enhance the scaling relationship of the intermediate and remarkably improve catalytic performance for the OER. The distinctive structural characteristics of microleaf arrays inhibit active particle agglomeration and offer an extensive specific surface area of 252.05 m^2 gm^{-1} for the reaction. The electrocatalyst performs superior high-current-density oxygen evolution, exhibiting a low overpotential (274 mV @ 1000 mA cm^{-2}) and Tafel slope (48.84 mV dec^{-1}).[151]

From the above discussion, it is clear that porous metal sulfides have shown promising potential as efficient electrocatalysts for water splitting, particularly in HER and OER in alkaline media. Combining these metal sulfides like MoS_2 and graphene can enhance their performance. Key findings include MoS_2-wrapped NiS_2 nanohybrids on graphene sheets exhibiting excellent bifunctional electrocatalytic activity, porous cobalt sulfides demonstrating superior catalytic activity and chemical stability, and heterostructured nanoelectrocatalysts such as CoS_2/CoS nanosheets and CoS_2/FeS-MOF enhancing intrinsic activity towards HER and OER. These findings underscore the potential of porous metal sulfides as effective electrocatalysts for water splitting.

5.2 Porous metal selenides for EWS

Selenide and sulfur are part of the same major group and exhibit numerous similarities in their properties. Metal selenides are exceptional electrocatalytic materials characterized by superior electrical conductivity and great physical density. Furthermore, the s and p orbitals of selenide can undergo hybridization with the d orbitals of metals, resulting in selenide exhibiting superior crystalline characteristics and catalytic efficacy. TMSe is anticipated to serve as a catalyst that can substitute precious metals due to its elevated catalytic activity, narrow band gap, excellent stability, and inexpensive cost.[152,153]

Porous metal selenides have several benefits, including facile synthesis, exceptional catalytic activity, and outstanding stability, which render them very suitable for water

This journal is © The Royal Society of Chemistry 2025

J. Mater. Chem. A, 2025, 13, 22271–22294 | 22283

electrochemical water-splitting.[154] Jiang et al.[155] created a structure consisting of nanoporous $Co_{0.85}Se$ with single-atom platinum (Pt/np-$Co_{0.85}Se$) to investigate the underlying factors contributing to the activity of the HER. The presence of atomic Pt in $Co_{0.85}Se$ optimizes the surface active sites, resulting in lower energy barriers and enhanced hydrogen adsorption/desorption. The combined action of Pt atoms and np-$Co_{0.85}Se$ resulted in an initial overpotential that was close to zero. The Tafel slope exhibited a remarkably low value of 35 mV dec^{-1}, while the turnover frequency reached an impressive value of 3.93 s^{-1} at -100 mV in a neutral solution. The diffusion of Pt ions into Co vacancies of nano-sized $Co_{0.85}Se$ ligaments is facilitated by the bicontinuous nanoporous structure with a large surface area (15.1 m^2 g^{-1}), creating the uniform Pt-doped np-$Co_{0.85}Se$ single-atom, which facilitated more efficient mass-transfer processes. These results surpassed those of commercial Pt/C.[155]

The creation of hierarchical nanostructures with very efficient and long-lasting multifunctional catalysts holds great importance in the realm of emerging water-splitting energy technologies. In this regard, Prabhakaran and colleagues[107] have shown a method for creating a 3D hierarchical structure of oxygenated cobalt molybdenum selenide (O-$Co_{1-x}Mo_xSe_2$) using nanoarchitectures. Following a facile and cost-effective hydrothermal method, these structures were fabricated using a one-of-a-kind ion exchange procedure (Fig. 7g).[107] At a relative pressure of 0.45 to 1.0, all materials displayed type IV isotherms with a hysteresis loop, indicating mesoporous characteristics. Above all, O-$Co_{0.5}Mo_{0.5}Se_2$ NSs had a huge specific surface area (SSA) of roughly 302 m^2 g^{-1}, significantly greater than that of O-$CoSe_2$ ($\approx$71 m^2 g^{-1}), O-$MoSe_2$ ($\approx$135 m^2 g^{-1}), O-$Co_{0.75}Mo_{0.25}Se_2$ ($\approx$186 m^2 g^{-1}), and O-$Co_{0.25}Mo_{0.75}Se_2$ ($\approx$225 m^2 g^{-1}). Furthermore, the O-$Co_{0.5}Mo_{0.5}Se_2$ NSs exhibit a mesoporous nature with an average pore size of around 3.59 nm. The oxygen released during the selenium process at 180 °C using a regulated ion-exchange approach is responsible for successfully developing the mesopores in the O-$Co_{0.5}Mo_{0.5}Se_2$ NSs. Due to its abundant electro-active sites and nanoporous networks, as well as its plentiful oxygen vacancies, the O-$Co_{0.5}Mo_{0.5}Se_2$ catalyst demonstrates efficient catalysis of the HER and OER (Fig. 7h). It achieves a low overpotential of approximately 102 and 189 mV, respectively, at a current density of 10 mA cm^{-2}. Additionally, it exhibits exceptional durability. The O-$Co_{0.5}Mo_{0.5}Se_2$‖O-$Co_{0.5}Mo_{0.5}Se_2$ water-splitting device requires a voltage of around 1.53 V at a current density of 10 mA cm^{-2} (Fig. 7i), which was significantly better than the benchmark Pt/C‖RuO$_2$ (approximately 1.56 V).[107]

Preparing improved three-dimensional electrodes and optimizing their morphology is crucial for increasing the electrocatalytic activity of catalysts. The catalytic activity is enhanced by directly depositing selenide onto a conductive substrate, reducing the resistance between the catalyst and the current collector. Nanofiber (NF) is frequently used as a substrate to create Ni–Co–Se nanostructures.[156,157] It simultaneously acts as both the framework and the source of Ni. The $Ni_{0.89}Co_{0.11}Se_2$ mesoporous nanosheet networks, developed by Liu et al.,[157] exhibit exceptional catalytic capabilities for the HER and

demonstrate remarkable stability throughout a broad pH range due to their distinctive morphology and electronic structure. The observation of a type IV isotherm with a hysteresis loop confirmed the mesoporous structure of the $Ni_{0.89}Co_{0.11}Se_2$ nanosheets. The specific surface area of $Ni_{0.89}Co_{0.11}Se_2$ nanosheets was determined to be 37.32 m^2 g^{-1}, and their mean pore size was 4.8 nm, ranging from 2 to 20 nm.[157] Poorahong et al.[149] have also fabricated a three-dimensional, binder-free bimetallic nickel–cobalt selenide nanosheet structure anchored on a macroporous conductive carbon membrane (NiCoSe$_2$@PCM). A distinctive interconnecting macroporous phase change material was synthesized using cryogelation, freeze-drying, and subsequent carbonization. The PCM serves as a framework for the development of a NiCoSe$_2$ catalyst (Fig. 7f). Uniform and compact nanosheets composed of few-layer NiCoSe$_2$ were synthesized on the surface of the PCM, eliminating the necessity for a transfer step or a conductive addition. The porous characteristic, as evidenced by the type IV isotherm, resulted in a high BET surface area of 38.2 m^2 g^{-1}. The NiCoSe$_2$ nanosheets, oriented perpendicularly, exhibit exceptional electrochemical catalytic activity, demonstrated by a low overpotential of 0.116 V (at 10 mA cm^{-2}) and a Tafel slope of 66 mV dec^{-1} for the HER, as well as an overpotential of 1.37 V (at 10 mA cm^{-2}) with a Tafel slope of 60 mV dec^{-1} for the OER. Remarkable stability with no degradation in current density was noted during a 23 hour testing duration. Bifunctional NiCoSe$_2$@PCM was used to construct a two-electrode electrolyzer, achieving 10 mA cm^{-2} at a low voltage of 1.73 V.

Wang et al.[158] have fabricated porous NiCo diselenide nanosheets on carbon cloth for water splitting. The NiCo diselenide nanosheets have a moderate BET-specific surface area (165 m^2 g^{-1}), which is about six times greater than that of Ni diselenide nanosheets (28 m^2 g^{-1}) but somewhat less than that of Co diselenide nanoplates (172 m^2 g^{-1}). The size distribution of nanopores on the surface of metal diselenide nanosheets may be related to the variation in BET surface area. Ni diselenide nanosheets have pores that are roughly 35 nm in size, which is more significant than that of Co diselenide nanoplates (5 nm) and NiCo diselenide nanosheets (8 nm). The NiCo diselenide/CC composites exhibited high HER activity with a small Tafel slope of 31.6 mV dec^{-1} and a low overpotential of 108 mV at 10 mA cm^{-2}. They also have superior OER capability with a small Tafel slope of 42.3 mV dec^{-1} and an OER current density of 10 mA cm^{-2} at a low potential of 258 mV. Their HER/OER activity remained steady even after 50 hours of polarization. The three-dimensional structure of the nanosheets facilitates the movement of charge and electrons, hence enhancing the availability of catalytic active sites.[158]

Recent studies have shown that metal selenides, specifically cobalt selenide ($Co_{0.85}Se$) and nickel–cobalt selenide (NiCoSe$_2$), can be effective water-splitting electrocatalysts. $Co_{0.85}Se$ exhibits exceptional HER activity with low overpotential and Tafel slope, while O-$Co_{1-x}MoxSe_2$ nanostructures demonstrate efficient HER and OER catalysis. NiCoSe$_2$ nanosheets anchored on conductive substrates show excellent electrochemical catalytic activity for HER and OER. The enhanced performance of these metal selenides can be attributed to their high surface area,

22284 | J. Mater. Chem. A, 2025, 13, 22271–22294

This journal is © The Royal Society of Chemistry 2025

Table 2 Electrochemical parameters of porous metal chalcogenides

Porous metal chalcogenides	Porosity	Electrolyte	OER η (mV) @ 10 mA cm^{-2}/Tafel slope	HER η (mV) @ 10 mA cm^{-2}/Tafel slope	Stability (h)	TOF (s^{-1}) @ 300 mV	Ref.
Ni_3S_2/MnS–O	Porous	1 M KOH	228/46	116/41	50	—	159
$Ni_{0.7}Fe_{0.3}S_2$	Porous	1 M KOH	198/56	155/109	13.8	—	160
h-Co_xS_y	Meso-	1 M KOH	320/98	295/145	18	0.45	161
N–Ni_3S_2/NF	Porous	1 M KOH	–/70	110	8	—	162
MoS_2/Mo	Macro-	0.5 M H_2SO_4	—	168/48	17	—	19
FeS_2	Meso-	0.1 M KOH	—	96/78	25	—	21
MoS_2–NiS_2/G	Meso-	0.5 M H_2SO_4	—	152/53	20	—	138
	Meso-	1 M KOH	320/82	141/77			
NiS_2	Meso-	0.5 M H_2SO_4	—	174/63	10	—	136
NiS	Meso-	1 M KOH	320/59	148/82			
MoNiFeS	Micro-	1 M KOH	190 @ 40/74.2	247 @ 40/164	50	—	163
$Zn_{0.5}Al_{0.5}S$@N-MC	Meso-	1 M KOH	340/23	—	50	—	164
NiCoPS@SC	Meso-	1 M KOH	329/87	—	12	—	165
$MoNiS_{3-x}O_x$	Porous	1 M KOH	—	231 @ 1 A/65.5	48	—	166
P-$CoNi_2S_4$	Porous	1 M KOH	282/40	135/65	100	—	147
MoS_2@$Zn_{0.76}Co_{0.24}S$	Meso-	1 M KOH	90 @ 20/57	169/39.7	48	—	167
$Ni_{0.76}Fe_{0.24}Se$	Meso-	1 M KOH	197/56	—	16.6	—	22
Pt/np-$Co_{0.85}Se$	Nano-	1 M PBS	—	55/35	40	3.93 @ 100 mV	155
$CuCo_2Se_4$@Au	Porous	1 M KOH	320 @ 50/66.5	125/-	8	0.041	168
$Ni_{0.89}Co_{0.11}Se_2$ MNSN/NF	Meso-	1 M KOH	189/62	85/52	30	—	157
O-$Co_{0.5}Mo_{0.5}Se_2$	Nano-	1 M KOH	—	102/59	36	—	107
N–$NiSe_2$/NF	Meso-	0.5 M H_2SO_4	—	102/	20	—	169
		1 M PBS		206			
		1 M KOH		86/69			
Fe-doped MOF CuCoSe@HCNF	Meso-	1 M KOH	260 @ 20/57	70/59	50	—	170
$Ni_{0.85}Se$/RGO	Porous	1 M KOH	320 @ 30/91	169/65	20	0.049	82
Co–ZnSe	Porous	1 M KOH	320/66	—	15	0.022	106
$NiSe_2$–$MoSe_2$@NC/CC	Porous	1 M KOH	280/84.4	91/63.6	70	—	171
CuTe-NS/NiF	Porous	0.5 M KOH	—	250/36	65	0.912 @ 350 mV	23
NiNCs-1T-Mn-VTe_2	Meso-	1 M KOH	258 @ 40/65.1	61/71.5	50	—	172
Co–Te NF	Porous	1 M KOH	241/201	90/143	15.5	1.03	134
Hollow $NiTe_2$	Meso-	0.5 M H_2SO_4	—	85/59	30	—	173
Fe-$Co_{1.11}Te_2$@NCNTF-2	Porous	1 M KOH	297/92	107/73	18	0.02	174
$CoTe_2$@NCNTFs	Meso-	1 M KOH	330/82.8	204/58.04	30	—	175
Fe-$Co_{1.11}Te_2$@NCNTF	Porous	1 M KOH	297/97.7	107/73	18	0.035	174

This journal is © The Royal Society of Chemistry 2025

J. Mater. Chem. A, 2025, **13**, 22271–22294 | **22285**

mesoporous structure, abundant electro-active sites, and optimized electronic structure (Table 2).

5.3 Porous metal tellurides for EWS

Porous metal tellurides (PMTs) have gained significant attention as new catalysts due to the unique properties of tellurium.[176–178] When compared to other chalcogens, such as selenium (Se) and sulfur (S), tellurium (Te) appears to have a lower electronegativity and a more robust metallic property.[115] This leads to increased electrical conductivity and a higher level of covalency in the metal–chalcogen links in PMTs. The presence of covalent character in the system can result in a beneficial electronic band structure. This makes it easier to align the edges of the valence band and the conduction band with the oxidation and reduction potentials of water that are present. In addition to this, it stimulates the redox reactions that occur within the transition metal center, which ultimately results in an improvement in the electrocatalytic performance.[23]

In reality, the gradual shift in the electronic band structure of oxides and the remainder of the chalcogenide series (sulfides, selenides, and tellurides) may explain the trend in catalytic activity between oxides and the rest of the chalcogenide series. This is because the margins of the valence and conduction bands coincide with the water oxidation–reduction levels.[179] As the electronegativity of the chalcogen atom falls further down the series, the degree of covalency in the metal–chalcogen bond increases. Previous research has shown that a higher degree of covalency in metal–anion bonding increases the efficiency of OER catalysis, so it is reasonable to expect the chalcogenide series to improve catalytic efficiency even more.[116] Because Te's electronegativity (2.1) is lower than Se's (2.55), nickel tellurides will have a higher degree of covalency than selenides. Indeed, a qualitative band structure investigation revealed that tellurides have a better band alignment with water oxidation levels than selenides. Gao et al.[115] synthesized innovative hierarchical $CoTe_2$ and CoTe nanofleeces for effective OER catalysts using phase-selective methods. The hierarchical $CoTe_2$ and CoTe nanofleeces exhibited BET surface areas of 97 and 75 m^2 g^{-1}, respectively, which are relatively high for transition metal chalcogenide materials. The elevated surface area is ascribed to the minuscule branched nanofleeces, which possess typical diameters of approximately 10 nm. At a modest overpotential of 357 mV, hierarchical $CoTe_2$ nanostructures have been claimed to be capable of achieving a current density of 10 mA cm^{-2} for the oxygen evolution reaction.[115]

Pan et al.[111] have developed nickel nanoclusters (NiNCs) that are combined with manganese (Mn) and inserted into and mixed with 1T VTe_2 nanosheets (NiNCs-1T-Mn-VTe_2 NS) to achieve EWS at extremely low potentials (Fig. 7j). The N_2 adsorption–desorption isotherm results indicated that NiNCs-1T-Mn-VTe_2 NS possesses the largest surface area of 92 m^2 g^{-1}, with an average pore diameter of 24.3 nm. The efficacy of EWS is greatly enhanced by Mn doping and intercalation in 1T VTe_2 (1T Mn VTe_2), as it improves the performances of both

the OER and the HER. Combining NiNCs with 1T Mn VTe_2 results in the formation of a very efficient electrochemical catalyst, known as NiNCs-1T-Mn-VTe_2 NS, to split water at extremely low potentials. The NiNCs-1T Mn VTe_2 NS exhibited remarkable performance, achieving a current density of 10 mA cm^2 with an HER overpotential of only 61 mV and a current density of 40 mA cm^2 with an OER overpotential of 258 mV. The NiNCs-1T Mn VTe_2 NS(+) device necessitated a cell potential of 1.51 V to achieve a current density of 10 mA cm^2 (Fig. 7k and l).[111]

The aforementioned study indicates that porous metal tellurides, particularly hierarchical $CoTe_2$ and CoTe nanofleeces, together with nickel nanoclusters integrated with manganese-doped VTe_2 nanosheets (NiNCs-1T-Mn-VTe_2 NS), serve as efficient electrocatalysts for water splitting. These nanostructures possess a high surface area and exhibit efficient catalytic activity for the OER, whereas NiNCs-1T-Mn-VTe_2 NS has outstanding performance in electrochemical water splitting, attaining low overpotentials for both reactions. The improved performance is due to elevated surface area, porosity, regulated doping and heterostructuring, diminished charge transfer resistance, and augmented electrical conductivity.

All the above-mentioned porous metal chalcogenides, including sulfides, selenides, and tellurides, exhibit discrete performances toward electrochemical water-splitting. The porous metal chalcogenide catalysts exhibit low overpotentials, achieve high current densities, and deliver high intrinsic activities. In addition, heterostructured chalcogenides with controlled doping can also help increase electrical conductivity by reducing charge transfer resistance. Despite the noticeable progress in a porous metal chalcogenides catalyst, the practical applications are still under development.

The correlation between the BET surface area and the HER and OER overpotential at 10 mA cm^{-2} of porous metal chalcogenides-based electrocatalysts is presented in Fig. 8. This analysis reveals a significant trend where high surface area porous metal chalcogenides exhibit substantially reduced overpotential values. Notably, the electrocatalysts $Ni_{0.5}Mo_{0.5}$-OSe, O-$Co_{0.5}Mo_{0.5}Se_2$, and V-$CoTe_2$/$MoTe_2$@CC, which possess high BET surface areas, demonstrate remarkably low overpotential values. This correlation suggests that the high surface area of these materials plays a crucial role in enhancing their electrocatalytic performance. Several benefits are associated with porous metal chalcogenides with a high surface area. These benefits include an increase in the number of active sites, an improvement in mass transport, and an enhancement in electrical conductivity. These characteristics allow for improved electron transport during electrochemical processes, reducing the constraints imposed by diffusion and enhancing the reaction's kinetics. The decreased overpotential values of these chalcogenides provide evidence that they have the potential to function as effective electrocatalysts for applications involving water splitting. Further optimization of their surface area, composition, and structure could lead to even more excellent performance and the development of energy storage and conversion technologies that are more efficient and sustainable.
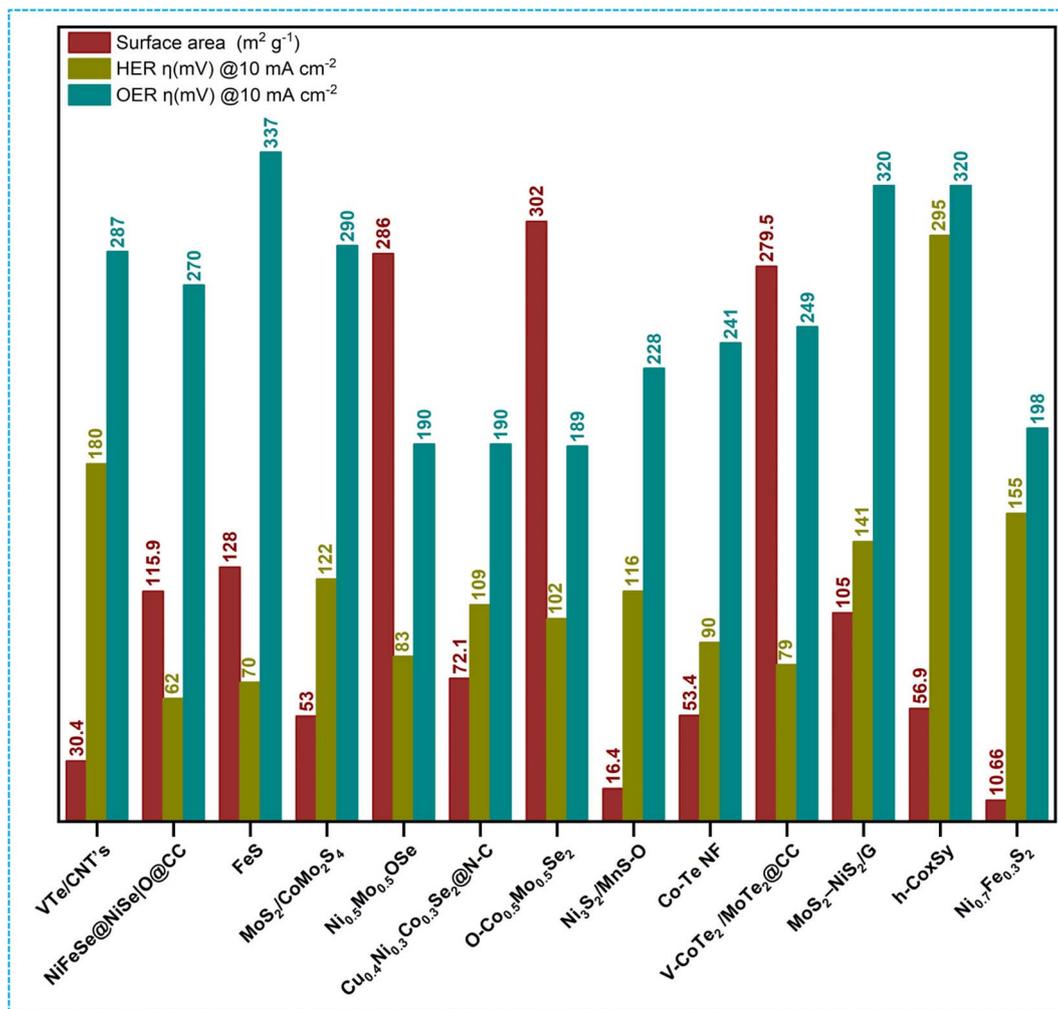
22286 | *J. Mater. Chem. A*, 2025, **13**, 22271–22294

This journal is © The Royal Society of Chemistry 2025

Fig. 8 The summary of the BET surface area, HER, and OER overpotential at 10 mA cm^{-2} of the various porous metal chalcogenides. The data were initially reported as follows: VTe/CNTs,[180] NiFeSe@NiSe/O@CC,[181] Ni$_{0.5}$Mo$_{0.5}$OSe,[104] MoS$_2$/CoMo$_2$S$_4$,[182] Cu$_{0.4}$Ni$_{0.3}$Co$_{0.3}$Se$_2$@N-C,[103] O-Co$_{0.5}$Mo$_{0.5}$Se$_2$,[107] Ni$_3$S$_2$/MnS-O,[159] CoTe NF,[110] V-CoTe$_2$/MoTe$_2$@CC,[113] MoS$_2$-NiS$_2$/G,[138] h-Co$_x$S$_y$,[161] Ni$_{0.76}$Fe$_{0.24}$Se.[22]

6. Performance of porous metal chalcogenides for overall water splitting

Water electrolyzers require an active catalyst to facilitate the HER and OER processes. Using a single OER and HER bifunctional electrocatalyst not only makes the entire system design easier but also reduces the cost of the system. One of the most challenging tasks is to drive the electrolyzer while maintaining a low cell voltage to achieve a high current density. To improve the overall water-splitting activity, it is of utmost significance to combine the advantages of HER and OER electrocatalysts to design OER-HER bifunctional heterostructures that are both long-lasting and effective.

In this regard, Pathak *et al.*[113] used a hydrothermal approach to synthesize a vanadium-doped cobalt/molybdenum precursor. During this process, the precursor was transformed into the matching telluride (Fig. 9a), which had the morphology of nanodendrites growing across 2D nanosheets (Fig. 9b and c).

Fig. 9d confirms that the N$_2$ adsorption isotherms of V-CoTe$_2$/MoTe$_2$@CC and CoTe$_2$/MoTe$_2$@CC exhibited typical type-IV isotherms. These isotherms had surface areas of 279.5 m^2 g^{-1} and 225.2 m^2 g^{-1}, respectively. BET studies demonstrated that the introduction of V doping into the material resulted in the formation of defects, lattice expansion, and surface roughening, all of which contributed to a considerable increase in the BET surface area. Furthermore, the BJH pore size distribution profiles of V-CoTe$_2$/MoTe$_2$@CC and CoTe$_2$/MoTe$_2$@CC demonstrate that the bulk of mesopores are approximately 5.5 nm and 5.1 nm, respectively. When it comes to aqueous alkaline electrolytes, the vast majority of mesopores are compatible with electrical mobility.

Importantly, comprehensive characterization shows how vanadium doping may be used to control the electrical characteristics of bimetallic tellurides. This is accomplished by causing lattice expansions and exposing ample active sites for the HER and OER. As a consequence of this, the V-CoTe$_2$/MoTe$_2$@CC material has remarkable performance in terms of
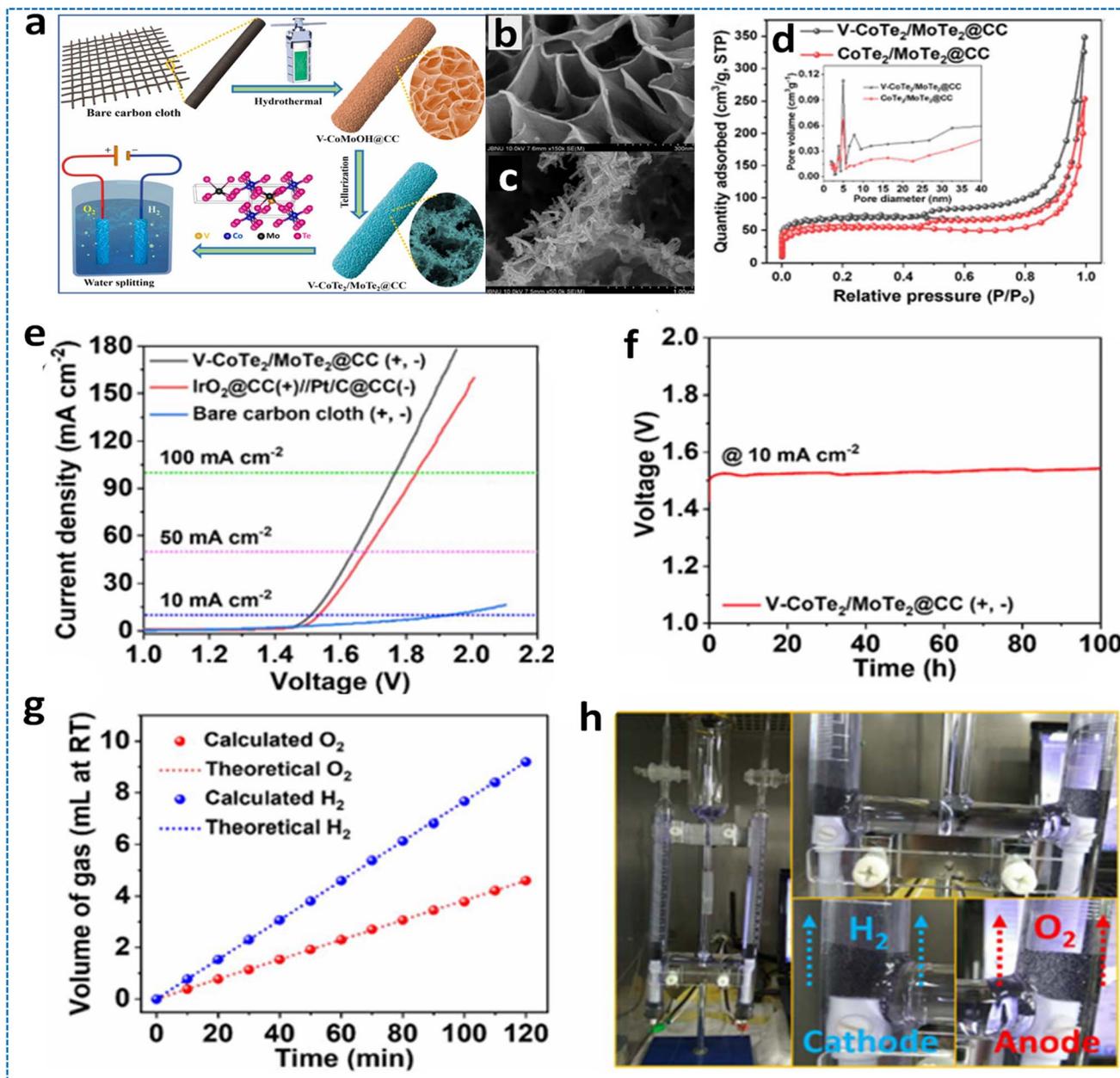
This journal is © The Royal Society of Chemistry 2025

J. Mater. Chem. A, 2025, **13**, 22271–22294 | **22287**

Fig. 9 (a) Schematic representation of the preparation of V-CoTe$_2$/MoTe$_2$@CC and its application for water splitting, (b) FESEM image of as-prepared V−CoMoOH@CC, (c) FESEM image of V-CoTe$_2$/MoTe$_2$@CC, (d) N$_2$ adsorption isotherms (inset: BJH pore size distribution profile), (e) polarization curves of V-CoTe$_2$/MoTe$_2$@CC(+, −), IrO$_2$@CC(+)//Pt/C@CC(−) and bare CC(+, −) devices, (f) chronopotentiometric stability test result at 10 mA cm^{-2}, (g) theoretical and experimental volumes of H$_2$ and O$_2$, (h) digital image of a laboratory-made H-cell set up for the measurement of faradaic efficiency (insets: enlarged photos showing the cathode and anode), generated at 10 mA cm^{-2} by the V-CoTe$_2$/MoTe$_2$@CC electrodes at varying times in an H-cell. Reproduced from ref. 113 with permission from Royal Society of Chemistry, copyright 2024.

both the HER ($\eta_{10} = 79$ mV, Tafel slope = 58.9 mV dec^{-1}) and the OER ($\eta_{10} = 249$ mV, Tafel slope = 57.7 mV dec^{-1}). In terms of overall water splitting, the V-CoTe$_2$/MoTe$_2$@CC(+, −) semiconductor beats the state-of-the-art IrO$_2$@CC(+)//Pt/C@CC(−) semiconductor (Fig. 9e). CoTe$_2$ and MoTe$_2$ are responsible for the synergistic effects that manifest themselves as a result of the modified lattice that is caused by vanadium dopants and the coexistence of several active sites.

Remarkably, the potential of the V-CoTe$_2$/MoTe$_2$@CC(+, −) full-cell device was demonstrated by continuously executing the

chronopotentiometry (CP) test for a duration of 100 hours at a current density of 10 mA cm^{-2} in a solution of 1.0 M KOH (Fig. 9f). The faradaic efficiency of the electrode materials was also investigated by measuring the volume of hydrogen and oxygen produced at a current density of 10 mA cm^{-2} at various time intervals using a laboratory-made hydrogen cell. The volume of hydrogen and oxygen produced was monitored every ten minutes for up to one hundred and twenty minutes. This was done to precisely match the theoretical values (Fig. 9g) and provide strong evidence of a one hundred percent faradaic

22288 | *J. Mater. Chem. A*, 2025, **13**, 22271–22294

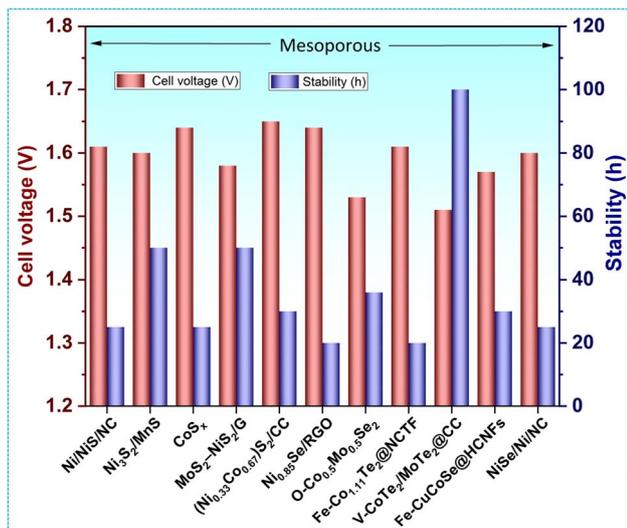This journal is © The Royal Society of Chemistry 2025

Fig. 10 Overall water-splitting cell voltage and stability of the bifunctional mesoporous metal chalcogenide electrocatalysts. The data were initially reported as follows: Ni/NiS/NC,[100] Ni_3S_2/MnS,[159] CoS_x,[101] MoS_2–NiS_2/G,[138] $(Ni_{0.33}Co_{0.67})S_2$/CC,[95] $Ni_{0.85}Se$/RGO,[82] O-$Co_{0.5}Mo_{0.5}Se_2$,[107] Fe-$Co_{1.11}Te_2$@NCTF,[174] V-$CoTe_2$/$MoTe_2$@CC,[113] Fe-CuCoSe@HCNFs,[170] and NiSe/Ni/NC.[183]

efficiency for the HER and the OER. The digital photos that are displayed in Fig. 9h show the H-cell electrolyzer that was manufactured in the laboratory, as well as the H_2 and O_2 bubbles that were produced at the cathode and anode, respectively.[113] Fig. 10 compares the overall water-splitting cell voltage and stability of the bifunctional mesoporous metal chalcogenide electrocatalysts. Several PMCh catalysts have exhibited superior performance in terms of their capacity to operate at low cell potential for overall water splitting. However, the issue of durability remains a concern. Fig. 10 depicts the V-$CoTe_2$/$MoTe_2$@CC catalyst, which is the most suitable choice for overall water splitting and practical application, demonstrating excellent performance and durability. Therefore, developing efficient bifunctional catalysts with long-lasting performance capable of being included in renewable technologies continues to be difficult.

In a nutshell, mesoporous metal chalcogenide materials exhibit exceptional efficacy in electrochemical water splitting owing to their distinctive structural and electrical characteristics. These materials possess larger pores (2–50 nm) compared to microporous materials, facilitating enhanced mass transfer of reactants and products during electrochemical processes. They possess an increased surface area, offering additional active sites for electrochemical reactions. Increased pore size diminishes diffusion constraints, facilitating easier access of reactants to active sites. Thus, mesoporous materials have enhanced electronic conductivity due to their reduced pore sizes. They demonstrate excellent stability compared to macroporous materials, which are susceptible to collapse or deterioration during electrochemical reactions. The pore structure can be adjusted to boost performance, and integrating metal and chalcogenide ions can improve the material's efficacy in water splitting.

7. Challenges and future research directions

A major challenge in utilizing PMChs for electrochemical water-splitting is the low electrical conductivity, restricted active areas, and inadequate stability under extreme operating conditions. Over time, PMChs often experience deterioration, resulting in reduced catalytic activity. Moreover, a substantial impediment must be addressed for the scalability of PMChs synthesis. Many researchers have investigated diverse techniques to tackle these challenges. Persistent efforts have demonstrated that these tactics will likely improve charge transfer and catalytic activity of PMChs. Nonetheless, additional research is required to resolve concerns of irreversible surface restoration. Surface modification can enhance the production of electrocatalytic hydroxyl oxide. Conversely, these hydroxyl oxides frequently dissolve in the electrolyte, leading to the corrosion of the catalyst or the degradation of its structure. Thus, achieving and sustaining the appropriate equilibrium during water splitting is essential for preserving the catalyst's efficacy. Fig. 11 depicts the major challenges and feasible solutions for the utilization of PMChs in electrochemical water-splitting applications.

(1) Porous metal chalcogenides are primarily manufactured using transition metals such as Co, Ni, Fe, *etc.* Additional metals such as indium (In), zinc (Zn), strontium (Sr), and others can be utilized in the synthesis of PMChs to augment their electrochemical capabilities further.

(2) Out of several cost-effective and easy synthesis methods, the hydrothermal reaction remains the most commonly employed technology. This simple synthesis approach requires very gentle reaction conditions compared to other procedures. Nevertheless, it presents challenges in monitoring crystal growth, limiting its applicability to laboratory settings and posing a significant obstacle to commercial use. Therefore, it is recommended that researchers develop a controlled and expandable synthetic method to produce different types of PMChs, as it is crucial for the widespread use of PMChs in industrial applications.

(3) The use of theoretical calculations employing Density Functional Theory (DFT) has been acknowledged as a potent method for obtaining significant insights into manipulating catalyst electronic structure and predicting the efficacy of new catalysts. Theoretical calculations offer insights into the crystal structure, electrical state, and chemical composition of PMChs. In addition, DFT provides valuable information on the process of introducing impurities (doping) and how the materials interact with polarizable molecular charge. These foundational understandings provide us with profound insight into the functioning mechanism of PMChs, as well as their activity and stability during electrolysis.

(4) The design of high-performance electrocatalysts is crucial for advancing energy storage and conversion technologies. Porous metal chalcogenides have shown great promise due to their unique structure and properties, but rational design remains a significant challenge. To address this, researchers
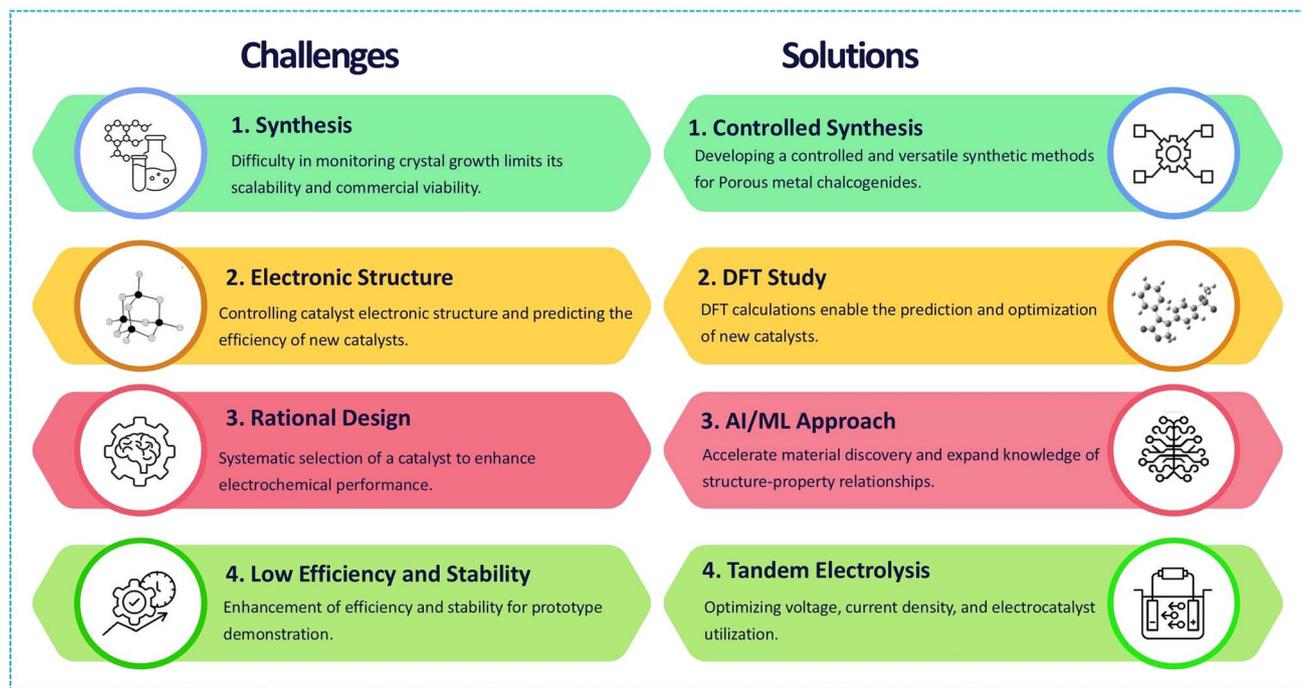
Challenges

1. Synthesis
Difficulty in monitoring crystal growth limits its scalability and commercial viability.

2. Electronic Structure
Controlling catalyst electronic structure and predicting the efficiency of new catalysts.

3. Rational Design
Systematic selection of a catalyst to enhance electrochemical performance.

4. Low Efficiency and Stability
Enhancement of efficiency and stability for prototype demonstration.

Solutions

1. Controlled Synthesis
Developing a controlled and versatile synthetic methods for Porous metal chalcogenides.

2. DFT Study
DFT calculations enable the prediction and optimization of new catalysts.

3. AI/ML Approach
Accelerate material discovery and expand knowledge of structure-property relationships.

4. Tandem Electrolysis
Optimizing voltage, current density, and electrocatalyst utilization.

Fig. 11 Schematic representation of the key challenges in utilizing porous metal chalcogenides for electrocatalytic water splitting and the corresponding feasible solutions.

recommend exploring the application of artificial intelligence (AI) and machine learning (ML) techniques to drive the design of porous metal chalcogenide electrocatalysts. By leveraging AI/ML algorithms, researchers can rapidly screen and optimize these materials' composition, structure, and properties to achieve enhanced electrocatalytic performance. By integrating AI/ML techniques into the design of porous metal chalcogenide electrocatalysts, researchers can unlock new opportunities for advancing energy storage and conversion technologies. The application of AI/ML techniques are expected to improve electrocatalytic performance significantly, reduce the time and resources required for experimental synthesis and testing, and provide a deeper understanding of structure–property relationships.

(5) Using porous metal chalcogenides as electrocatalysts for electrochemical water splitting is promising for producing clean hydrogen fuel. However, further improvements are needed to achieve high efficiency and stability. Tandem electrolysis, which involves using two or more electrochemical cells connected in series, can enhance the efficiency and stability of the water-splitting process. Tandem electrolysis can improve efficiency by optimizing voltage and current density for each cell, reducing the risk of electrode degradation and enhancing stability. It also allows for greater flexibility in designing water-splitting systems by enabling the use of different electrocatalysts and operating conditions. Porous metal chalcogenides offer high surface areas, enabling enhanced electrochemical reaction rates and efficiency, making them suitable for tandem electrolysis.

(6) Porous metal chalcogenides' distinctive structure and characteristics make them highly promising electrocatalysts for electrochemical water splitting. However, additional enhancements are required to reach a state of great utility. Therefore, it may be feasible to implement hybrid processes that integrate photocatalysis with bio-electrochemical systems or other water splitting methods. Increased efficiency, stability, sustainability, and cost-effectiveness are possible advantages of hybrid processes. The increased surface areas of porous metal chalcogenides allow for more efficient and rapid electrochemical reactions. Their tunable properties can be fine-tuned to optimize particular hybrid processes by manipulating their structure, morphology, and composition. Porous metal chalcogenides are well-suited for hybrid processes due to their long-term stability and performance in electrochemical applications. Building and optimizing hybrid processes that integrate different water splitting methods with electrocatalysts based on porous metal chalcogenides, creating new porous metal chalcogenide materials with enhanced hybrid process capabilities, and finally, commercializing and scaling up hybrid processes utilizing porous metal chalcogenides are all areas that could benefit from further research in the future.

8. Conclusions

Pursuing cost-effective, highly efficient, and stable electrocatalysts is crucial for promoting energy conversion through electrocatalytic reactions. PMCh electrocatalysts have emerged as a promising option for catalyzing electrochemical reactions.

22290 | *J. Mater. Chem. A*, 2025, **13**, 22271–22294

This journal is © The Royal Society of Chemistry 2025

These catalysts possess porous structure, inherent activity, a regulated electronic structure, and a specific composition, making them highly effective in achieving this objective. The distinctive characteristics of porous metal chalcogenide nanomaterials, including optimal atomic configuration, superior electrical conductivity, easily modifiable structure, and scalability in synthesis, have significant implications for research across various domains. Innovative materials, various synthetic processes, and improved methodologies have been developed to synthesize porous metal chalcogenide nanocrystals to provide more active and stable metal sulfide-based nanomaterials. Furthermore, hybrid engineering with metal chalcogenides facilitates the creation of innovative functional composites with various materials, including metals, oxides, nitrides, chalcogenides, and carbides.

This article provides a detailed analysis of the progress in developing PMCh electrocatalysts. These catalysts have enhanced performance in terms of HER and OER, leading to better overall efficiency in water splitting. This paper comprehensively explains the rational methods used to build PMCh electrocatalysts to achieve improved efficiency in overall water splitting and related processes. The paper also discussed several synthesis methods for creating porous structures with distinct morphologies. Despite several investigations conducted using experimental techniques, PMChs continue to provide significant promise in advancing the efficiency of the water-splitting process.

Recent research has investigated the potential of PMCh as a catalyst for enhancing performance in water electrolysis. Although there are significant obstacles to overcome, it is anticipated that the current research endeavors in manufacturing, *in situ* characterization, theoretical computation, modeling, and experimentation will lead to advancements in PMCh electrocatalysts that can be implemented on an industrial scale.

Data availability

All data for this manuscript are available and obtained from the corresponding author.

Conflicts of interest

The authors declare that they have no known competing financial interests or personal relationships that could have appeared to influence the work reported in this paper.

References

1 N. S. Lewis and D. G. Nocera, *Proc. Natl. Acad. Sci. U. S. A.*, 2006, **103**, 15729–15735.
2 E. A. Quadrelli, G. Centi, J.-L. Duplan and S. Perathoner, *ChemSusChem*, 2011, **4**, 1194–1215.
3 P. Poizot and F. Dolhem, *Energy Environ. Sci.*, 2011, **4**, 2003–2019.
4 S. Sikiru, T. L. Oladosu, T. I. Amosa, J. O. Olutoki, M. Ansari, K. J. Abioye, Z. U. Rehman and H. Soleimani, *Int. J. Hydrogen Energy*, 2024, **56**, 1152–1182.
5 X. Li, L. Zhao, J. Yu, X. Liu, X. Zhang, H. Liu and W. Zhou, *Nano-Micro Lett.*, 2020, **12**, 1–29.
6 S. Anantharaj, P. E. Karthik, B. Subramanian and S. Kundu, *ACS Catal.*, 2016, **6**, 4660–4672.
7 K. A. Stoerzinger, O. Diaz-Morales, M. Kolb, R. R. Rao, R. Frydendal, L. Qiao, X. R. Wang, N. B. Halck, J. Rossmeisl and H. A. Hansen, *ACS Energy Lett.*, 2017, **2**, 876–881.
8 P. M. Bodhankar, P. B. Sarawade, G. Singh, A. Vinu and D. S. Dhawale, *J. Mater. Chem. A*, 2021, **9**, 3180–3208.
9 P. M. Bodhankar, D. S. Dhawale, S. Giddey, R. Kumar and P. B. Sarawade, *Sustainable Energy Fuels*, 2022, **6**, 5491–5502.
10 P. M. Bodhankar, P. B. Sarawade, P. Kumar, A. Vinu, A. P. Kulkarni, C. D. Lokhande and D. S. Dhawale, *Small*, 2022, **18**, 2107572.
11 P. M. Bodhankar, A. Chunduri, N. Patel, D. S. Dhawale, A. Vinu, H. Aljohani and P. B. Sarawade, *Sustainable Energy Fuels*, 2021, **5**, 1120–1128.
12 Y. Jin, H. Wang, J. Li, X. Yue, Y. Han, P. K. Shen and Y. Cui, *Adv. Mater.*, 2016, **28**, 3785–3790.
13 W. Li, H. Yao, K. Yan, G. Zheng, Z. Liang, Y.-M. Chiang and Y. Cui, *Nat. Commun.*, 2015, **6**, 7436.
14 Y. Liu, Y. Guo, Y. Liu, Z. Wei, K. Wang and Z. Shi, *Energy Fuels*, 2023, **37**, 2608–2630.
15 D. Gao, B. Xia, C. Zhu, Y. Du, P. Xi, D. Xue, J. Ding and J. Wang, *J. Mater. Chem. A*, 2018, **6**, 510–515.
16 L. Yang, L. Huang, Y. Yao and L. Jiao, *Appl. Catal., B*, 2021, **282**, 119584.
17 H. Xu, J. Cao, C. Shan, B. Wang, P. Xi, W. Liu and Y. Tang, *Angew. Chem.*, 2018, **130**, 8790–8794.
18 W. Wang, H. Cao, W. Li, J. Wu, E. Sheng, Z. Chen, W.-C. Cheong and K. Wu, *Mater. Lett.*, 2020, **272**, 127828.
19 Z. Pu, Q. Liu, A. M. Asiri, Y. Luo, X. Sun and Y. He, *Electrochim. Acta*, 2015, **168**, 133–138.
20 Y. Jiang, S. Gao, J. Liu, G. Xu, Q. Jia, F. Chen and X. Song, *Nanoscale*, 2020, **12**, 11573–11581.
21 R. Miao, B. Dutta, S. Sahoo, J. He, W. Zhong, S. A. Cetegen, T. Jiang, S. P. Alpay and S. L. Suib, *J. Am. Chem. Soc.*, 2017, **139**, 13604–13607.
22 J. Yu, G. Cheng and W. Luo, *Nano Res.*, 2018, **11**, 2149–2158.
23 Q. U. Khan, M. W. Ishaq, N. Begum, K. Khan, U. Khan, A. T. Khan, M. A. U. Din, M. Idrees and L. Zhu, *Int. J. Hydrogen Energy*, 2021, **46**, 18729–18739.
24 J. Yin, J. Jin, H. Lin, Z. Yin, J. Li, M. Lu, L. Guo, P. Xi, Y. Tang and C. H. Yan, *Adv. Sci.*, 2020, **7**, 1903070.
25 I. Vamvasakis, K. S. Subrahmanyam, M. G. Kanatzidis and G. S. Armatas, *ACS Nano*, 2015, **9**, 4419–4426.
26 C. Gu, H.-M. Xu, S.-K. Han, M.-R. Gao and S.-H. Yu, *Chem. Soc. Rev.*, 2021, **50**, 6671–6683.
27 T. D. C. Ha, H. Lee, I. Vamvasakis, G. S. Armatas, Y. Oh and M. G. Kim, *EcoMat*, 2023, **5**, e12419.
28 S. Bag and M. G. Kanatzidis, *J. Am. Chem. Soc.*, 2010, **132**, 14951–14959.
29 S. Bag, I. U. Arachchige and M. G. Kanatzidis, *J. Mater. Chem.*, 2008, **18**, 3628–3632.
30 Z. Hassanzadeh Fard, S. M. Islam and M. G. Kanatzidis, *Chem. Mater.*, 2015, **27**, 6189–6192.

This journal is © The Royal Society of Chemistry 2025

J. Mater. Chem. A, 2025, **13**, 22271–22294 | **22291**

31 J. Zhao, J. Wang, Z. Chen, J. Ju, X. Han and Y. Deng, *APL Mater.*, 2021, **9**, 050902.

32 C. H. Hendon, K. T. Butler, A. M. Ganose, Y. Román-Leshkov, D. O. Scanlon, G. A. Ozin and A. Walsh, *Chem. Mater.*, 2017, **29**, 3663–3670.

33 H. Mu, G. Lin, Y. Zhang, Y. Xiao and J. Liu, *Colloids Surf., A*, 2021, **623**, 126734.

34 K. S. Sing, *Pure Appl. Chem.*, 1985, **57**, 603–619.

35 S. Polarz and B. Smarsly, *J. Nanosci. Nanotechnol.*, 2002, **2**, 581–612.

36 W. Luc and F. Jiao, *ACS Catal.*, 2017, **7**, 5856–5861.

37 G. Wittstock, M. Bäumer, W. Dononelli, T. Klüner, L. Lührs, C. Mahr, L. V. Moskaleva, M. Oezaslan, T. Risse, A. Rosenauer, A. Staubitz, J. Weissmüller and A. Wittstock, *Chem. Rev.*, 2023, **123**, 6716–6792.

38 S. De, J. Zhang, R. Luque and N. Yan, *Energy Environ. Sci.*, 2016, **9**, 3314–3347.

39 A. Kumari, S. Kaushal and P. P. Singh, *Mater. Today Energy*, 2021, **20**, 100667.

40 Z. Wei, J. Sun, Y. Li, A. K. Datye and Y. Wang, *Chem. Soc. Rev.*, 2012, **41**, 7994–8008.

41 J. Zhang and C. M. Li, *Chem. Soc. Rev.*, 2012, **41**, 7016–7031.

42 C. Perego and R. Millini, *Chem. Soc. Rev.*, 2013, **42**, 3956–3976.

43 G. Singh, J. Lee, A. Karakoti, R. Bahadur, J. Yi, D. Zhao, K. AlBahily and A. Vinu, *Chem. Soc. Rev.*, 2020, **49**, 4360–4404.

44 H. Chen, X. Liang, Y. Liu, X. Ai, T. Asefa and X. Zou, *Adv. Mater.*, 2020, **32**, 2002435.

45 K. A. Adegoke and N. W. Maxakato, *Coord. Chem. Rev.*, 2022, **457**, 214389.

46 T. J. Barton, L. M. Bull, W. G. Klemperer, D. A. Loy, B. McEnaney, M. Misono, P. A. Monson, G. Pez, G. W. Scherer and J. C. Vartuli, *Chem. Mater.*, 1999, **11**, 2633–2656.

47 J. Qi, W. Zhang and R. Cao, *ChemCatChem*, 2018, **10**, 1206–1220.

48 L. Kong, M. Zhong, W. Shuang, Y. Xu and X.-H. Bu, *Chem. Soc. Rev.*, 2020, **49**, 2378–2407.

49 X.-Y. Yang, L.-H. Chen, Y. Li, J. C. Rooke, C. Sanchez and B.-L. Su, *Chem. Soc. Rev.*, 2017, **46**, 481–558.

50 A. H. Lu and F. Schüth, *Adv. Mater.*, 2006, **18**, 1793–1805.

51 P. Sinha, A. Datar, C. Jeong, X. Deng, Y. G. Chung and L.-C. Lin, *J. Phys. Chem. C*, 2019, **123**, 20195–20209.

52 S. Brunauer, P. H. Emmett and E. Teller, *J. Am. Chem. Soc.*, 1938, **60**, 309–319.

53 K. S. Sing, *Adsorption by Powders and Porous Solids*, 2013, vol. 2, pp. 237–268.

54 U. Kuila and M. Prasad, *Lead. Edge*, 2013, **32**, 1478–1485.

55 N. Rameli, K. Jumbri, R. Wahab, A. Ramli and F. Huyop, 2018.

56 L. Zhang, L. Jin, B. Liu and J. He, *Front. Chem.*, 2019, **7**, 22.

57 A. Eftekhari, *Microporous Mesoporous Mater.*, 2017, **243**, 355–369.

58 J. Širc, R. Hobzova, N. Kostina, M. Munzarová, M. Juklíčková, M. Lhotka, Š. Kubinová, A. Zajícová and J. Michálek, *J. Nanomater.*, 2012, **2012**, 327369.

59 F. Yu, H. Zhou, Y. Huang, J. Sun, F. Qin, J. Bao, W. A. Goddard III, S. Chen and Z. Ren, *Nat. Commun.*, 2018, **9**, 2551.

60 A. Kumar and S. Bhattacharyya, *ACS Appl. Mater. Interfaces*, 2017, **9**, 41906–41915.

61 S. Chen and S.-Z. Qiao, *ACS Nano*, 2013, **7**, 10190–10196.

62 F. Jamal, A. Rafique, S. Moeen, J. Haider, W. Nabgan, A. Haider, M. Imran, G. Nazir, M. Alhassan and M. Ikram, *ACS Appl. Nano Mater.*, 2023, **6**, 7077–7106.

63 H. Liang, L. Li, F. Meng, L. Dang, J. Zhuo, A. Forticaux, Z. Wang and S. Jin, *Chem. Mater.*, 2015, **27**, 5702–5711.

64 Y. Hou, M. Qiu, T. Zhang, X. Zhuang, C. S. Kim, C. Yuan and X. Feng, *Adv. Mater.*, 2017, **29**, 1701589.

65 S. Roy, A. Joseph, X. Zhang, S. Bhattacharyya, A. B. Puthirath, A. Biswas, C. S. Tiwary, R. Vajtai and P. M. Ajayan, *Chem. Rev.*, 2024, **124**, 9376–9456.

66 Y. Liu, P. Vijayakumar, Q. Liu, T. Sakthivel, F. Chen and Z. Dai, *Nano-Micro Lett.*, 2022, **14**, 43.

67 J. Yin, J. Jin, H. Lin, Z. Yin, J. Li, M. Lu, L. Guo, P. Xi, Y. Tang and C.-H. Yan, *Adv. Sci.*, 2020, **7**, 1903070.

68 Y. Zhang, Q. Zhou, J. Zhu, Q. Yan, S. X. Dou and W. Sun, *Adv. Funct. Mater.*, 2017, **27**, 1702317.

69 K. Mensah-Darkwa, D. Nframah Ampong, E. Agyekum, F. M. de Souza and R. K. Gupta, *Energies*, 2022, **15**, 4052.

70 L. Yu, J. F. Yang and X. W. Lou, *Angew. Chem.*, 2016, **128**, 13620–13624.

71 B. Y. Guan, L. Yu, X. Wang, S. Song and X. W. Lou, *Adv. Mater.*, 2016, **29**, 1605051.

72 W. Wang, L. Kuai, W. Cao, M. Huttula, S. Ollikkala, T. Ahopelto, A. P. Honkanen, S. Huotari, M. Yu and B. Geng, *Angew. Chem.*, 2017, **129**, 15173–15177.

73 J. Zhu, L. Hu, P. Zhao, L. Y. S. Lee and K.-Y. Wong, *Chem. Rev.*, 2019, **120**, 851–918.

74 Y. Yao, Z. Zhang and L. Jiao, *Energy Environ. Mater.*, 2022, **5**, 470–485.

75 F. Lyu, Q. Wang, S. M. Choi and Y. Yin, *Small*, 2019, **15**, 1804201.

76 Y. H. Budnikova, *Dalton Trans.*, 2020, **49**, 12483–12502.

77 J. Tafel, *Z. Phys. Chem., Stoechiom. Verwandtschaftsl.*, 1905, **50**, 641–712.

78 X.-P. Li, C. Huang, W.-K. Han, T. Ouyang and Z.-Q. Liu, *Chin. Chem. Lett.*, 2021, **32**, 2597–2616.

79 X. Zou and Y. Zhang, *Chem. Soc. Rev.*, 2015, **44**, 5148–5180.

80 A. Yadav, Y. Hunge and S.-W. Kang, *Surf. Interfaces*, 2021, **23**, 101020.

81 H. Su, J. Jiang, S. Song, B. An, N. Li, Y. Gao and L. Ge, *Chin. J. Catal.*, 2023, **44**, 7–49.

82 G. Liu, C. Shuai, Z. Mo, R. Guo, N. Liu, X. Niu, Q. Dong, J. Wang, Q. Gao and Y. Chen, *New J. Chem.*, 2020, **44**, 17313–17322.

83 Y. Guo, J. Tang, Z. Wang, Y.-M. Kang, Y. Bando and Y. Yamauchi, *Nano Energy*, 2018, **47**, 494–502.

84 Y. Guo, T. Park, J. W. Yi, J. Henzie, J. Kim, Z. Wang, B. Jiang, Y. Bando, Y. Sugahara and J. Tang, *Adv. Mater.*, 2019, **31**, 1807134.

85 W. Li, J. Liu and D. Zhao, *Nat. Rev. Mater.*, 2016, **1**, 1–17.

22292 | *J. Mater. Chem. A*, 2025, **13**, 22271–22294

This journal is © The Royal Society of Chemistry 2025

86 A. Fischereder, M. L. Martinez-Ricci, A. Wolosiuk, W. Haas, F. Hofer, G. Trimmel and G. J. Soler-Illia, *Chem. Mater.*, 2012, **24**, 1837–1845.

87 B. T. Yonemoto, G. S. Hutchings and F. Jiao, *J. Am. Chem. Soc.*, 2014, **136**, 8895–8898.

88 Y. Shi, Y. Wan, R. Liu, B. Tu and D. Zhao, *J. Am. Chem. Soc.*, 2007, **129**, 9522–9531.

89 C. R. Lubeck, T. J. Han, A. E. Gash, J. H. Satcher Jr and F. M. Doyle, *Adv. Mater.*, 2006, **18**, 781–784.

90 P. N. Trikalitis, K. K. Rangan, T. Bakas and M. G. Kanatzidis, *Nature*, 2001, **410**, 671–675.

91 P. N. Trikalitis, K. K. Rangan and M. G. Kanatzidis, *J. Am. Chem. Soc.*, 2002, **124**, 2604–2613.

92 J. L. Mohanan, I. U. Arachchige and S. L. Brock, *Science*, 2005, **307**, 397–400.

93 F. Gao, Q. Lu and D. Zhao, *Adv. Mater.*, 2003, **15**, 739–742.

94 Y. Wang, Y. Wu, A. Shirazi-Amin, P. Kerns, J. Fee, J. He, L. Jin, R. Maric and S. L. Suib, *ACS Appl. Energy Mater.*, 2019, **2**, 2370–2374.

95 Q. Zhang, C. Ye, X. L. Li, Y. H. Deng, B. X. Tao, W. Xiao, L. J. Li, N. B. Li and H. Q. Luo, *ACS Appl. Mater. Interfaces*, 2018, **10**, 27723–27733.

96 X. Ma, W. Zhang, Y. Deng, C. Zhong, W. Hu and X. Han, *Nanoscale*, 2018, **10**, 4816–4824.

97 Z. Wang, J. Li, X. Tian, X. Wang, Y. Yu, K. A. Owusu, L. He and L. Mai, *ACS Appl. Mater. Interfaces*, 2016, **8**, 19386–19392.

98 S. Wan, W. Jin, X. Guo, J. Mao, L. Zheng, J. Zhao, J. Zhang, H. Liu and C. Tang, *ACS Sustain. Chem. Eng.*, 2018, **6**, 15374–15382.

99 Z. Chen, M. Chen, X. Yan, H. Jia, B. Fei, Y. Ha, H. Qing, H. Yang, M. Liu and R. Wu, *ACS Nano*, 2020, **14**, 6968–6979.

100 J. Ding, S. Ji, H. Wang, H. Gai, F. Liu, V. Linkov and R. Wang, *Int. J. Hydrogen Energy*, 2019, **44**, 2832–2840.

101 H. Bian, T. Chen, Z. Chen, J. Liu, Z. Li, P. Du, B. Zhou, X. Zeng, J. Tang and C. Liu, *Electrochim. Acta*, 2021, **389**, 138786.

102 Y. Guo, J. Tang, J. Henzie, B. Jiang, W. Xia, T. Chen, Y. Bando, Y.-M. Kang, M. S. A. Hossain, Y. Sugahara and Y. Yamauchi, *ACS Nano*, 2020, **14**, 4141–4152.

103 H. Hosseini and M. Roushani, *Chem. Eng. J.*, 2020, **402**, 126174.

104 J. Balamurugan, T. T. Nguyen, D. H. Kim, N. H. Kim and J. H. Lee, *Appl. Catal., B*, 2021, **286**, 119909.

105 Z.-t. Shang, T.-m. Li, B.-q. Hu, M. Liu, W.-t. Lu, F. Yu and Y. Zheng, *Front. Energy*, 2024, **18**, 378–389.

106 G. Fang, Q. Wang, J. Zhou, Y. Lei, Z. Chen, Z. Wang, A. Pan and S. Liang, *ACS Nano*, 2019, **13**, 5635–5645.

107 S. Prabhakaran, J. Balamurugan, N. H. Kim and J. H. Lee, *Small*, 2020, **16**, 2000797.

108 K. Srinivas, F. Ma, Y. Liu, Z. Zhang, Y. Wu and Y. Chen, *ACS Appl. Mater. Interfaces*, 2022, **14**, 52927–52939.

109 K. Chandra Majhi, P. Karfa and R. Madhuri, *Electrochim. Acta*, 2019, **318**, 901–912.

110 L. Nisar, M. Sadaqat, A. Hassan, N.-U.-A. Babar, A. Shah, M. Najam-Ul-Haq, M. N. Ashiq, M. F. Ehsan and K. S. Joya, *Fuel*, 2020, **280**, 118666.

111 U. N. Pan, D. R. Paudel, A. Kumar Das, T. I. Singh, N. H. Kim and J. H. Lee, *Appl. Catal., B*, 2022, **301**, 120780.

112 Y. R. Rosyara, A. Muthurasu, K. Chhetri, I. Pathak, T. H. Ko, P. C. Lohani, D. Acharya, T. Kim, D. Lee and H. Y. Kim, *ACS Appl. Mater. Interfaces*, 2024, **16**, 10238–10250.

113 I. Pathak, A. Muthurasu, D. Acharya, K. Chhetri, B. Dahal, Y. R. Rosyara, T. Kim, T. H. Ko and H. Y. Kim, *J. Mater. Chem. A*, 2024, **12**, 17544–17556.

114 K. M. Katubi, M. U. Nisa, S. Manzoor, Z. Ahmad, A. G. Abid, M. Abdullah, M. S. Al-Buriahi and M. N. Ashiq, *Appl. Phys. A:Mater. Sci. Process.*, 2022, **128**, 882.

115 Q. Gao, C. Q. Huang, Y. M. Ju, M. R. Gao, J. W. Liu, D. An, C. H. Cui, Y. R. Zheng, W. X. Li and S. H. Yu, *Angew. Chem., Int. Ed.*, 2017, **56**, 7769–7773.

116 J. Masud, P. C. Ioannou, N. Levesanos, P. Kyritsis and M. Nath, *ChemSusChem*, 2016, **9**, 3128–3132.

117 F. A. Rasmussen and K. S. Thygesen, *J. Phys. Chem. C*, 2015, **119**, 13169–13183.

118 Z. Xue, X. Li, Q. Liu, M. Cai, K. Liu, M. Liu, Z. Ke, X. Liu and G. Li, *Adv. Mater.*, 2019, **31**, 1900430.

119 J. Xu, Y. Yin, H. Xiong, X. Du, Y. Jiang, W. Guo, Z. Wang, Z. Xie, D. Qu and H. Tang, *Appl. Surf. Sci.*, 2019, **490**, 516–521.

120 F. M. Sapountzi, J. M. Gracia, C. J. Weststrate, H. O. A. Fredriksson and J. W. Niemantsverdriet, *Prog. Energy Combust. Sci.*, 2017, **58**, 1–35.

121 S. Wang, A. Lu and C.-J. Zhong, *Nano Convergence*, 2021, **8**, 4.

122 P. J. Megía, A. J. Vizcaíno, J. A. Calles and A. Carrero, *Energy Fuels*, 2021, **35**, 16403–16415.

123 B. You and Y. Sun, *Acc. Chem. Res.*, 2018, **51**, 1571–1580.

124 S. Anwar, F. Khan, Y. Zhang and A. Djire, *Int. J. Hydrogen Energy*, 2021, **46**, 32284–32317.

125 K. Mazloomi and C. Gomes, *Renewable Sustainable Energy Rev.*, 2012, **16**, 3024–3033.

126 Y. Wu, B. Xiao, K. Liu, S. Wang, Y. Hou, X. F. Lu and J. Zhang, *Electrochem. Energy Rev.*, 2025, **8**, 2.

127 Y. Hua, H. Jiang, H. Jiang, H. Zhang and C. Li, *Electrochim. Acta*, 2018, **278**, 219–225.

128 K. Pan, Y. Zhai, J. Zhang and K. Yu, *Materials*, 2019, **12**, 3364.

129 L. Tong, C. Song, Y. Liu, R. Xing, K. Sekar and S. Liu, *Int. J. Hydrogen Energy*, 2022, **47**, 14404–14413.

130 L. Zhang, J. Rong, Y. Lin, Y. Yang, H. Zhu, X. Yu, X. Kang, C. Chen, H. M. Cheng and G. Liu, *Adv. Funct. Mater.*, 2023, **33**, 2307947.

131 B. Chen, P. Hu, F. Yang, X. Hua, F. F. Yang, F. Zhu, R. Sun, K. Hao, K. Wang and Z. Yin, *Small*, 2023, **19**, 2207177.

132 A. Wang, K. Hu, Y. Liu, R. Li, C. Ye, Z. Yi and K. Yan, *Int. J. Hydrogen Energy*, 2019, **44**, 6573–6581.

133 X. Wang, X. Huang, W. Gao, Y. Tang, P. Jiang, K. Lan, R. Yang, B. Wang and R. Li, *J. Mater. Chem. A*, 2018, **6**, 3684–3691.

134 L. Nisar, M. Sadaqat, A. Hassan, A. Shah, M. Najam-Ul-Haq, M. N. Ashiq, M. F. Ehsan and K. S. Joya, *Fuel*, 2020, **280**, 118666.

This journal is © The Royal Society of Chemistry 2025

J. Mater. Chem. A, 2025, **13**, 22271–22294 | **22293**

135 F. Wang, Y. Li, T. A. Shifa, K. Liu, F. Wang, Z. Wang, P. Xu, Q. Wang and J. He, *Angew. Chem., Int. Ed.*, 2016, **55**, 6919–6924.

136 L. Pan, Z. Huijuan, L. Li, Z. Yan, D. Ju, X. Chaohe, H. Ning and W. Yu, *ACS Appl. Mater. Interfaces*, 2017, **9**, 2500–2508.

137 J.-T. Ren and Z.-Y. Yuan, *ACS Sustain. Chem. Eng.*, 2017, **5**, 7203–7210.

138 S. P. Lonkar, V. V. Pillai and S. M. Alhassan, *Mater. Adv.*, 2020, **1**, 794–803.

139 Y. Yang, M. Yuan, H. Li, G. Sun and S. Ma, *Electrochim. Acta*, 2018, **281**, 198–207.

140 X. Luo, Q. Zhou, S. Du, J. Li, J. Zhong, X. Deng and Y. Liu, *ACS Appl. Mater. Interfaces*, 2018, **10**, 22291–22302.

141 Y. Li, X. Fu, W. Zhu, J. Gong, J. Sun, D. Zhang and J. Wang, *Inorg. Chem. Front.*, 2019, **6**, 2090–2095.

142 P. Cai, J. Huang, J. Chen and Z. Wen, *Angew. Chem.*, 2017, **129**, 4936–4939.

143 L. Lei, D. Huang, C. Zhang, R. Deng, S. Chen and Z. Li, *J. Catal.*, 2020, **385**, 129–139.

144 G. Zhao, K. Rui, S. X. Dou and W. Sun, *Adv. Funct. Mater.*, 2018, **28**, 1803291.

145 X. Luo, P. Ji, P. Wang, R. Cheng, D. Chen, C. Lin, J. Zhang, J. He, Z. Shi, N. Li, S. Xiao and S. Mu, *Adv. Energy Mater.*, 2020, **10**, 1903891.

146 Y. Li, W. Wang, B. Huang, Z. Mao, R. Wang, B. He, Y. Gong and H. Wang, *J. Energy Chem.*, 2021, **57**, 99–108.

147 X. F. Lu, S. L. Zhang, W. L. Sim, S. Gao and X. W. Lou, *Angew. Chem.*, 2021, **133**, 23067–23073.

148 X. Hu, P. Tan, R. Dong, M. Jiang, L. Lu, Y. Wang, H. Liu, Y. Liu, J. Xie and J. Pan, *Energy Technol.*, 2021, **9**, 2000961.

149 S. Poorahong, D. J. Harding, S. Keawmorakot and M. Siaj, *J. Electroanal. Chem.*, 2021, **897**, 115568.

150 Y. Yang, Q. Zhou, J. Yang, D. Qian, Y. Xiong, Z. Li and Z. Hu, *Int. J. Hydrogen Energy*, 2022, **47**, 33728–33740.

151 B. Zhao, H. Luo, J. Liu, S. Chen, H. Xu, Y. Liao, X. F. Lu, Y. Qing and Y. Wu, *Chin. Chem. Lett.*, 2025, **36**, 109919.

152 Z. Wang, S. Liu, W. Duan, Y. Xing, Y. Hu and Y. Ma, *Int. J. Hydrogen Energy*, 2024, **60**, 1414–1432.

153 X. Xia, L. Wang, N. Sui, V. L. Colvin and W. W. Yu, *Nanoscale*, 2020, **12**, 12249–12262.

154 M. Mushtaq, M. Koroma, S. Jiang, S. Mathi, M. Tu, Z. Khanam, Y.-W. Hu, J. Deng and M.-S. Balogun, *J. Mater. Chem. A*, 2025, **13**, 5933–5944.

155 K. Jiang, B. Liu, M. Luo, S. Ning, M. Peng, Y. Zhao, Y.-R. Lu, T.-S. Chan, F. M. de Groot and Y. Tan, *Nat. Commun.*, 2019, **10**, 1743.

156 K. Xiao, L. Zhou, M. Shao and M. Wei, *J. Mater. Chem. A*, 2018, **6**, 7585–7591.

157 B. Liu, Y. F. Zhao, H. Q. Peng, Z. Y. Zhang, C. K. Sit, M. F. Yuen, T. R. Zhang, C. S. Lee and W. J. Zhang, *Adv. Mater.*, 2017, **29**, 1606521.

158 X. Wang, Y. Zheng, J. Yuan, J. Shen, J. Hu, A.-j. Wang, L. Wu and L. Niu, *Electrochim. Acta*, 2017, **225**, 503–513.

159 Y. Zhang, J. Fu, H. Zhao, R. Jiang, F. Tian and R. Zhang, *Appl. Catal., B*, 2019, **257**, 117899.

160 J. Yu, G. Cheng and W. Luo, *J. Mater. Chem. A*, 2017, **5**, 15838–15844.

161 Z. Zhang, S. Li, X. Bu, Y. Dai, J. Wang, X. Bao and T. Wang, *New J. Chem.*, 2021, **45**, 17313–17319.

162 P. Chen, T. Zhou, M. Zhang, Y. Tong, C. Zhong, N. Zhang, L. Zhang, C. Wu and Y. Xie, *Adv. Mater.*, 2017, **29**, 1701584.

163 B. Ranjith, L. Gnanasekaran, P. C. Karthika, J. R. Rajabathar, H. A. Al-Lohedan, W. K. Kim, V. R. M. Reddy, M. Kapoor, S. Singh, M. Lavanyaj and G. Devendrapandi, *Int. J. Hydrogen Energy*, 2025, **112**, 255–265.

164 S. Shah, K. Jabbour, M. Abdullah, A. T. Alfagham, A. M. Elgorban, M. F. Ehsan and M. U. Nisa, *J. Korean Ceram. Soc.*, 2025, **52**, 1–10.

165 Y. Zhang, T. Yu, J. Zhou, D. Li, M. Feng, Z. Zhang, Q. Yao and Y. Zhou, *Korean J. Chem. Eng.*, 2025, **42**, 857–866.

166 C. Shi, J. Zhou, M. A. Boda, K. Zhao, Z. Yang, D. Yuan and Z. Yi, *J. Mater. Chem. A*, 2025, **13**, 4538–4549.

167 M. M. Meshesha, J. Gautam, D. Chanda, S. G. Jang and B. L. Yang, *J. Colloid Interface Sci.*, 2023, **652**, 272–284.

168 X. Cao, J. E. Medvedeva and M. Nath, *ACS Appl. Energy Mater.*, 2020, **3**, 3092–3103.

169 F. Jing, Q. Lv, Q. Wang, K. Chi, Z. Xu, X. Wang and S. Wang, *Electrochim. Acta*, 2019, **304**, 202–209.

170 S.-H. Chae, A. Muthurasu, T. Kim, J. S. Kim, M.-S. Khil, M. Lee, H. Kim, J. Y. Lee and H. Y. Kim, *Appl. Catal., B*, 2021, **293**, 120209.

171 H. Zhou, D. Kong, N. Chu, H. Wang, J. Xu, Y. Wang and T. Xu, *J. Colloid Interface Sci.*, 2025, **678**, 968–976.

172 U. N. Pan, D. R. Paudel, A. K. Das, T. I. Singh, N. H. Kim and J. H. Lee, *Appl. Catal., B*, 2022, **301**, 120780.

173 F. Zhang, T.-y. Eom, M. Cho, H.-J. Lee and H. Pang, *J. Energy Storage*, 2021, **42**, 103098.

174 B. He, X. C. Wang, L. X. Xia, Y. Q. Guo, Y. W. Tang, Y. Zhao, Q. L. Hao, T. Yu, H. K. Liu and Z. Su, *ChemSusChem*, 2020, **13**, 5239–5247.

175 X. Wang, X. Huang, W. Gao, Y. Tang, P. Jiang, K. Lan, R. Yang, B. Wang and R. Li, *J. Mater. Chem. A*, 2018, **6**, 3684–3691.

176 K. S. Bhat, H. C. Barshilia and H. Nagaraja, *Int. J. Hydrogen Energy*, 2017, **42**, 24645–24655.

177 M. Sadaqat, L. Nisar, F. Hussain, M. N. Ashiq, A. Shah, M. F. Ehsan, M. Najam-Ul-Haq and K. S. Joya, *J. Mater. Chem. A*, 2019, **7**, 26410–26420.

178 M. Nath, U. De Silva, H. Singh, M. Perkins, W. P. Liyanage, S. Umapathi, S. Chakravarty and J. Masud, *ACS Appl. Energy Mater.*, 2021, **4**, 8158–8174.

179 Y. Xu and M. A. Schoonen, *Am. Mineral.*, 2000, **85**, 543–556.

180 N. Bano, S. Manzoor, A. Sami, S. I. A. Shah, A. Junaid, M. Y. U. Rehman, R. A. Alshgari, M. F. Ehsan and M. N. Ashiq, *J. Am. Ceram. Soc.*, 2024, **107**, 4027–4041.

181 M. Singh, T. T. Nguyen, J. Balamurugan, N. H. Kim and J. H. Lee, *Chem. Eng. J.*, 2022, **430**, 132888.

182 Y. Guo, J. Tang, J. Henzie, B. Jiang, W. Xia, T. Chen, Y. Bando, Y.-M. Kang, M. S. A. Hossain and Y. Sugahara, *ACS Nano*, 2020, **14**, 4141–4152.

183 J. Ding, P. Wang, S. Ji, H. Wang, D. J. Brett and R. Wang, *Electrochim. Acta*, 2019, **300**, 93–101.

22294 | *J. Mater. Chem. A*, 2025, **13**, 22271–22294

This journal is © The Royal Society of Chemistry 2025